CHALMERS
UNIVERSITY OF TECHNOLOGY

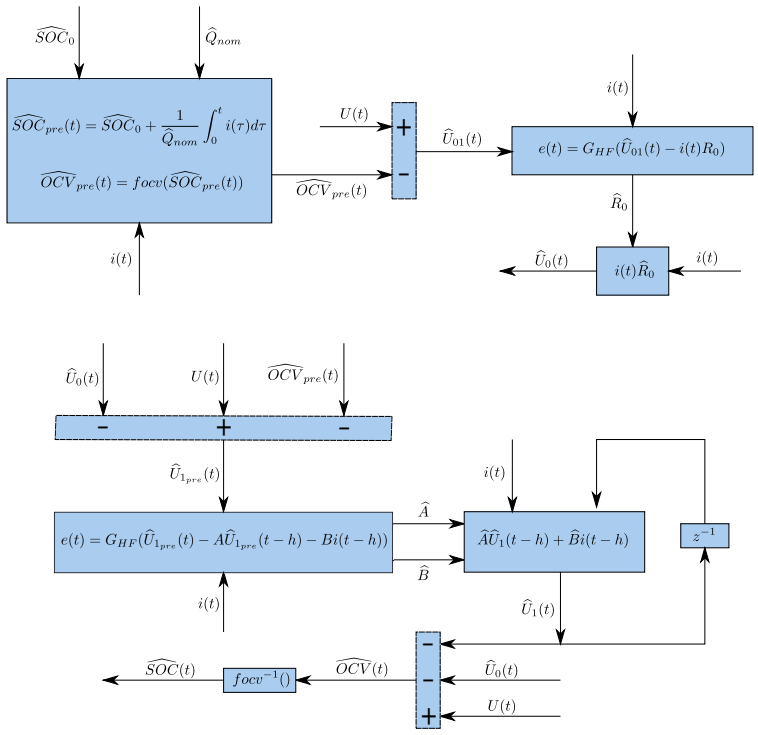


# On-line Algorithms for Detecting and Isolating Electrical Errors in High-Voltage Battery Packs

## An investigation of the internal short circuit and detection strategies with and without short circuit resistance estimation

Master's thesis in Electric Power Engineering

CHANDRASEKHAR NAGARAJ

Department of Electrical Engineering
CHALMERS UNIVERSITY OF TECHNOLOGY
Gothenburg, Sweden 2019

Master's thesis 2019:EENX30

# On-line Algorithms for Detecting and Isolatinng Electrical Errors in High-Voltage Battery Packs

An investigation of the internal short circuit and detection strategies with and without short circuit resistance estimation

CHANDRASEKHAR NAGARAJ


CHALMERS
UNIVERSITY OF TECHNOLOGY

Department of Electrical Engineering
*Division of Electric Power Engineering*
Chalmers University of Technology
Gothenburg, Sweden 2019

On-line Algorithms for Detecting and Isolating Electrical Errors in High-Voltage Battery Packs
An investigation of the internal short circuit and detection strategies with and without short circuit resistance estimation
CHANDRASEKHAR NAGARAJ



Supervisor: Christian Fleischer, Volvo Cars
Examiner: Torbjörn Thiringer, Department of Electrical Engineering

Master's Thesis 2019:EENNX30
Department of Electrical Engineering
Division of Electric Power Engineering
Chalmers University of Technology
SE-412 96 Gothenburg
Telephone +46 31 772 1000

Cover: *SOC* and parameter estimation procedure.

Typeset in LaTeX
Gothenburg, Sweden 2019

On-line Algorithms for Detecting and Isolating Electrical Errors in High-Voltage Battery Packs
An investigation of the internal short circuit and detection strategies with and without short circuit resistance estimation
CHANDRASEKHAR NAGARAJ
Department of Electrical Engineering
Chalmers University of Technology

# Abstract

Battery technology has gained significant attention in recent years due to the electric vehicle revolution. Safety is an important concern for stakeholders, with several reported incidents of thermal runaway. In this work, fault detection algorithms are designed and evaluated for various levels of the internal short circuit in a battery cell. A plant model of the battery cell and pack are designed for fault simulation both in Simulink and Simscape. A comparative analysis based detection strategy is first evaluated where estimated open circuit voltage is the metric for comparison. Satisfactory detection is observed with this technique for various intensities of the internal short circuit. A second method for detecting abnormal self-discharge using a linear fit on terminal voltage measurements is also evaluated. Finally, a state of charge and parameter estimator is developed using frequency separation and used for estimating the short circuit resistance. Capacity of the cell is also estimated using this methodology. The estimates obtained are observed to be close to the actual values used in the plant model, thus enabling monitoring of the intensity of internal short.

**Keywords**: Battery, logical cell, individual cell, state of charge, open circuit voltage, internal short circuit, short circuit resistance, recursive least squares, forgetting factor, parameter estimation

# Acknowledgements

This thesis work was conducted at Volvo Cars in Gothenburg, Sweden from January to May 2019.

I would first like to thank my supervisor at Volvo Cars, Christian Fleischer for his technical and moral support in conducting this work. He has been very patient and helpful whenever I was faced with challenges in various aspects of this work and always went out of his way to make sure they were solved. I also express heartfelt thanks to Marcus Hedegärd at Volvo Cars who offered invaluable support with his sharp insights, technical command and helpful nature. It was solely his ability to think outside the box that made overcoming many technical barriers possible.

I am grateful to my examiner at Chalmers, Torbjörn Thiringer for his patience and support with respect to providing valuable feedback on the report and answering questions. I also thank Zeyang Geng at Chalmers for her support.

Morover, I would like to thank all the members of the Traction Battery Controls and Calibration team that were extremely helpful despite their busy schedules. They made the whole experience meaningful and treated me like family.

Finally, I would like to recognize the precious support of family and friends, without which this work wouldn't have been possible.

Chandrasekhar Nagaraj, Gothenburg, May 2019

# Contents

# 1
# Introduction

In recent years, the interest towards electric and hybrid vehicles have risen sharply [1], with lithium-ion batteries gaining prominence as the energy source [2]. The driving factors for their widespread usage is attributed to their energy density, power density, reliability and long life [2] which proves to be very promising. However, safety remains a crucial issue to be addressed [3], and there have been several reported accidents such as the fire in a Boeing 787-8 aircraft [4], and battery failures in Samsung Note 7 [5]. Thus, there is an imminent need to develop fault detection techniques that can offer reliable indications ahead of time so a hazardous incident is thwarted.

The most common reason behind thermal runaway in a battery has been identified as internal short circuit (ISCr) [6], although other reasons such as chemical crossover [7] can also result in a thermal runaway. This project, however, will focus on the modeling and detection of an ISCr in a battery cell due to its widespread nature. There can be several possible factors that lead to the short circuit in a battery, such as defects in manufacturing [8], overcharge [9] or overdischarge [10].

There have been several techniques proposed in literature for fault detection in a battery pack. Some methodologies are not model based and use either additional measuring equipment or special tests to detect abnormal self-discharge. In one such method, a fault is both detected and isolated from electrical current measurements at the terminals of a battery pack with multiple parallel strings [11]. Another method proposes installing multiple sensors with different response speeds and reliability for definitive fault detection [12]. A third method uses the self-discharge current as the metric and estimates it through a dedicated test [13]. In this project, however, model based fault diagnosis schemes will be investigated as it offers many inherent benefits such as low cost and increased flexibility [14]. Furthermore, inaccuracies in the model can be handled with some observer-based estimation techniques [14].

In the model based detection camp, several possible approaches to fault detection have been proposed. These can further be broadly characterized into methods that use the internal short circuit resistance ($R_{ISCr}$) as a fault metric and ones that do not. The former set of methods is typically used under operating constraints such as evaluating faults in a cell without information from other cells in a battery pack or availability of only the battery pack terminal voltage without individual voltages of cells. In techniques without $R_{ISCr}$ calculation, the method observed to be most promising in the context of this project work involves evaluating consistency of es-

timated open circuit voltage/internal resistance between different series-connected cells in a battery pack [15], which offers accurate detection. Another method uses combined estimated parameters of an equivalent circuit model (ECM) and an energy balance equation (EBE) model in order to detect a fault [16]. This technique offers detection of a nascent or instantaneous ISCr, and is robust w.r.t location of the fault in the battery cell. However, verification of this algorithm was done for only one current profile and it is unsure if reliable parameter variation will be obtained with other profiles. Some other methods involve Multiple Model Adaptive Estimation (MMAE) algorithms that use several models simulating the healthy state and various fault conditions, and corresponding Extended Kalman Filters (EKF) for each condition [17], [18]. The residuals from the multiple EKFs are assessed to determine likelihoods of the battery being in one of the states. This method has the obvious disadvantage of being computationally intensive and also, the number of fault conditions considered might not be exhaustive. Electrochemical model based detection methods have also been proposed [19], but complexity can be a crucial issue with such techniques.

To give a brief overview of methods attempted using the $R_{ISCr}$ as a metric, a model is typically used in combination with various measurements for estimation. For instance, in methods proposed in [20], [21], voltage and current measurements of individual cells are employed to estimate the Open Circuit Voltage (OCV) and State of Charge (SOC) of the faulted cell using which the $R_{ISCr}$ is calculated. Another method estimates the faulty cell $R_{ISCr}$ in a battery pack using voltage measurements of the entire pack along with an equivalent circuit model of the pack with the EKF algorithm [22], but it is observed to be less accurate. All of these methods are observed to be prone to errors and unreliable estimation. In this project work, in addition to methods for identifying faults without identifying $R_{ISCr}$, a novel method of estimating the $R_{ISCr}$ and the capacity of the cell using a high-pass filter is proposed, analyzed and evaluated in simulation.

The following sections describe the aim and scope of this project in context of the material presented above.

## 1.1 Aim

The aim of this project is to simulate and detect faults in a battery pack. Once a battery model is implemented for simulating faults, various algorithms for fault detection will be designed an evaluated for performance.

## 1.2 Scope

- In this work, a battery model will first be built for fault simulation. The electrical faults considered here are mechanisms that occur in the cell, modeled as abnormal self-discharge. Other possible electrical errors that can occur in the

cell are not considered.

- A fault detection technique on the same lines as [15] will be developed in MATLAB/Simulink to detect instantaneous faults, following which a second method will be developed to monitor long term self-discharge effects. Both these methods will not estimate the value of $R_{ISCr}$, and would merely employ a comparative analysis over cells of the battery pack.

- A recursive parameter and state of charge estimator will then be developed using a high pass filter to filter out low frequency errors in the estimation loop, following which the capacity of the cell and $R_{ISCr}$ can be estimated using the SOC estimate. The estimation for the $R_{ISCr}$ and capacity will not be recursive, and will simply use data over the entire driving window to estimate those entities. Furthermore, the tuning parameters such as the initial covariance and forgetting factor will not be optimized formally in this work but chosen through trial and error and other reasonable considerations.

- The algorithms developed will be tested in simulation environment for driving profiles that are chosen appropriately to present performance. Verification of the algorithms with experimentally obtained data will not be performed.

- The sustainable aspects relevant to this project will be discussed with respect to ecological, economic and social dimensions.

- A few chosen ethical aspects from the IEEE code of ethics will also be discussed in relevance to this work.

## 1.3 Outline

The body of this thesis report is organized into a theory chapter, that describes the relevant theoretical background necessary for the analyses presented in this project work. This is followed by a method chapter, that highlights the principles of implementation of fault simulation and detection algorithms. A chapter on results then follows to present the outcome of the proposed detection schemes. A short discussion then ensues to highlight uncertainties in the work and provide further commentary on the results followed by a conclusion.

# 2
# Theory

In the following sections, the theoretical background relevant for this project is presented. First, a description of the battery model employed is described followed by a discussion of the internal short circuit simulation. Subsequently, the theoretical background necessary for an understanding of the detection algorithms is presented.

## 2.1 The lithium-ion battery

In this section, an overview of the chemistry of the lithium-ion (Li-ion) battery and relevant important definitions are presented. A battery is an energy storage device (ESD), and the Li-ion battery is of the rechargeable kind that can be charged and discharged many times. The Li-ion battery consists of a cathode, e.g. $LiFePO_4$ (LFP), an anode, e.g. Graphite, a separator and an electrolyte which is a lithium salt in an organic solvent [23]. The potential difference between the electrodes drives current to flow when an external load is applied across the cell terminals.

The discharge process of the Li-ion battery involves release of Lithium (Li) ions and electrons (oxidation) at the negative electrode, and the reverse mechanism (reduction) at the positive electrode. The Li-ions are conducted through the electrolyte from the negative to the positive electrode and the electrons flow through an external circuit into the positive electrode. Thus, current flows from the cathode to the anode of the battery during discharge. The exact opposite occurs during charging of the battery.

It is important to mention that a typical battery pack in an electric/hybrid vehicle consists of several individual battery cells. In this work, the term 'battery cell' or 'cell' will be used to describe the individual cell, while 'battery pack' will refer to an arrangement of several individual cells.

Before proceeding further with the subject of this project work, it is important to briefly discuss the a few concepts related to batteries.

### 2.1.1 State of Charge ($SOC$)

The state of charge is used as an indicator of the extent of 'fullness' of the battery in terms of the ratio of the available charge (residual capacity) to the maximum possi-

ble charge that can be drawn from the battery in the fully charged state (maximum available capacity). The residual and maximum available capacity of the battery are expressed typically in $Ampere - hour$ (Ah) units, and the $SOC$ can subsequently be expressed as a percentage.

The maximum available capacity of the battery depends on temperature, aging extent of the battery and discharge rate [24]. In this work however, these effects on the capacity shall not be considered.

### 2.1.2 Open circuit voltage ($OCV$)

The $OCV$ of a battery cell is the difference between its terminals in the absence of an electric load (no-load). The $OCV$ typically varies non-linearly with the $SOC$ for a lithium-ion battery, and laboratory experiments have been designed to quantify this relationship [25].

It is important to note that the $OCV$ of a battery changes with temperature and age [26], but these effects shall not be considered in this study. Furthermore, $OCV$ hysteresis is a well documented phenomenon [27] where the $OCV$-$SOC$ relationship is slightly different for charge and discharge. The average of the two $OCV$ profiles is usually considered for the $SOC$-$OCV$ function/look-up table in simulations.

### 2.1.3 Polarization in a battery cell

When an electric current flows through the battery, the terminal voltage of the cell deviates from equilibrium. This is referred to as polarization and may occur at the cathode or the anode of the cell. There are three different mechanisms for polarization during electric current flow [28].

- *Activation/Charge transfer polarization* is associated with the charge transfer reaction occurring at the surface of the electrodes. In order to overcome the energy barrier of the slowest step of a reaction, an overpotential is observed and is the activation polarization.

- *Concentration/Diffusion polarization* is associated with the potential difference observed as a consequence of varying ion concentration near the electrode surface.

- *Resistance polarization* is the ohmic potential drop across the electrodes, electrolyte, separator and the metal contact terminals of the cell.

The above mentioned effects can be captured in equivalent circuit models (ECMs) through use of various components, chosen with considerations of accuracy and complexity.

## 2.2 The battery cell equivalent circuit

In this section, the equivalent circuit of the battery cell relevant to this project shall be discussed. The important battery definitions from Section 2.1 must be kept in hindsight for a comprehensive understanding of the modeling.

### 2.2.1 Healthy cell

An Equivalent Circuit Model (ECM) of the battery cell was provided at the start of the project, and the entire battery pack consists of several cells described by the same ECM. The ECM used is a first order model (Thevenin model) [29] consisting of an open circuit voltage, internal resistance and a polarization branch as shown in Figure 2.1.

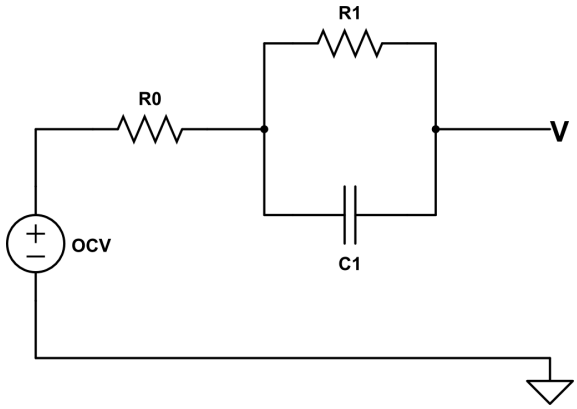


**Figure 2.1:** First-order Equivalent circuit model

In Figure 2.1, $OCV$ represents the open circuit voltage of the cell that typically varies with it's state of charge ($SOC$) non-linearly, $R_0$ represents the electrolyte resistance in the cell and $R_1$, $C_1$ represent the polarization resistance and capacitance respectively [29]. $V$ is the terminal voltage that can be measured across the cell.

#### 2.2.1.1 Characterization and parameter identification

The parameters in an equivalent circuit are not fixed quantities but vary with $SOC$, temperature and other factors thus requiring characterization with respect to these entities. In addition, there are other characteristics of a cell such as capacity and $OCV$-$SOC$ curve etc which also must be identified. Several tests can be performed on a cell towards this purpose. Some of them are the charge-discharge test, the electrochemical impedance spectroscopy (EIS) test and the current pulse test [30].

The charge-discharge tests involve charging and discharging an electrochemical energy storage device at various current rates, using which the capacity and $OCV$-$SOC$ profile can be obtained. EIS tests are used to acquire the frequency dependence of a component's impedance which can subsequently be used for ECM parameter estimation. The current pulse test applies a current pulse input to the component and

measures the voltage response using which parameters are identified. The EIS and current pulse tests can be applied at various temperature and $SOC$ levels, thereby enabling parameter estimation under various conditions.

### 2.2.2 Faulty cell

As mentioned before, the primary reason for thermal runaway in a battery is internal short circuit (ISCr) [6]. This fault can simply be represented as an additional parallel resistance $R_{ISCr}$ across the terminals of the ECM shown in Figure 2.1. This is reasonable because the characteristics of an ISCr and external short circuit are observed to be quite similar [31]. This modification results in the circuit in Figure 2.2.

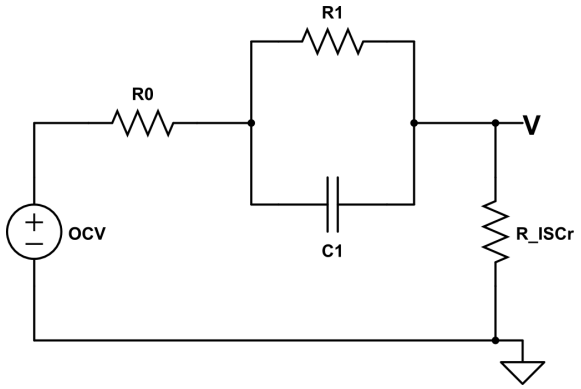


**Figure 2.2:** ECM with $R_{ISCr}$

Different intensities of the fault Various are represented by changing the value of $R_{ISCr}$. In an ideal healthy cell, $R_{ISCr}$ is large and during occurrence of a fault, the value is much smaller. As the intensity of the fault increases, the value of $R_{ISCr}$ decreases. Studies have been performed to identify critical levels of $R_{ISCr}$ that represent a transition from a 'soft' short to a 'hard' short, with some research suggesting a critical value of 10 Ω below which a thermal runaway might occur [16]. In this work, several values of $R_{ISCr}$ will be used to perform simulations and identification.

## 2.3 The battery cell discrete time model

In this section, the discrete time models for the healthy and faulted battery cell presented in Section 2.2 shall be described. Before proceeding to the actual cells, the discrete time system equation for an RC link is derived. In continuous time, the voltage across the RC link can be expressed as

$$\dot{V} = \frac{-V}{R_1 C_1} + \frac{I}{C_1}. \tag{2.1}$$

Discretization of (2.1) yields

$$V(k+1) = AV(k) + BI(k) \tag{2.2a}$$

$$A = e^{GT} \quad , \quad B = (A-1)HG^{-1} \tag{2.2b}$$

$$G = \frac{-1}{R_1 C_1} \quad , \quad H = \frac{1}{C_1} \tag{2.2c}$$

where T is the sampling time and the $A$ and $B$ matrices, and subsequently the $G$ and $H$ matrices for the discrete time system are expressed in terms of $R$ and $C$.

### 2.3.1 Healthy cell

In a healthy cell ECM shown in Figure 2.1, the terminal voltage can be expressed as a sum of the $OCV$, voltage drop across $R_0$ and voltage drop across the polarization RC link ($V_1$) as

$$V_t(k) = OCV(k) + I(k)R_0 + V_1(k) \tag{2.3a}$$

$$V_1(k) = \phi V_1(k-1) + R(1-\phi)I(k-1) \tag{2.3b}$$

where $\phi$ is defined as $e^{\frac{-T}{RC}}$ after simplifying (2.2). Also, the current $I$ is considered positive during charging in (2.3). In (2.3a), the $OCV(k)$ can be obtained from the state of charge $SOC(k)$, as there is a non-linear relationship between the two in lithium-ion batteries [25]. The $SOC(k)$ in turn can be obtained from coulomb counting in discrete time, which is essentially counting charge entering/leaving the battery. If the coulomb efficiency is considered to be 100 %, the $SOC$ at a time instant $k$ can be written as

$$SOC(k) = SOC(k-1) + I(k-1)\frac{T}{Q_{nom}} \tag{2.4}$$

where $Q_{nom}$ is the nominal capacity of the battery and T is the sampling time.

### 2.3.2 Faulty cell

As described in section 2.2.2, a cell with an internal short (see Figure 2.2) can be modeled as a healthy cell with an external resistance $R_{ISCr}$ across its terminals. As a consequence, the current through the cell $I(k)$ is obtained by subtracting the load current at a certain time instant $I_L(k)$ with the short circuit current ($I_{SCr}$) through the $R_{ISCr}$. This is observed easily from Figure 2.2 and can be written as

$$I(k) = I_L(k) - \frac{V_t(k)}{R_{ISCr}} \tag{2.5}$$

In order to model a fault, (2.5) is used as an expression for the current trough the cell in (2.3). However, usage of $V_t(k)$ to calculate $V_t(k)$ itself results in an algebraic

loop in the model and to work around this effect, an earlier sample $V_t(k-1)$ is chosen instead. This is a reasonable approximation as the sample time is small in the simulations and the difference between successive values of the terminal voltage are observed to be quite small.

The discrete-time model mentioned above is first implemented in Simulink to simulate faults and check the performance of the fault detection algorithm to gauge its viability, and also because computational time using a Simulink model is smaller than Simscape - which shall be described shortly. The actual battery pack to be analyzed consists of logical cell units that have three cells in parallel, with several such logical cells in series. Simulation of such a system is very difficult in Simulink, and therefore, Simscape shall be used to model this system.

## 2.4 Simscape modeling

Simscape is used for modeling of physical systems in the Simulink environment. Physical models of the components in the system can be chosen either from predefined components available in the library, or can be coded to suit custom user demands. The various components can then be connected easily in the system, as connections are made for physical signals and not data like in Simulink. However, integration to Simulink blocks can also be accomplished through data conversion blocks, thus making the modeling process convenient.

Simscape is an acausal modelling tool, which means that inputs and outputs need not be specified explicitly between components and instead, are inferred from the solutions to the equations. Furthermore, the same model structure can be re-used across physical simulations without making major changes. The implementation of a battery cell will be described in the Methods section.

## 2.5 Least squares and robust least squares

The least squares is a non-recursive parameter estimation technique, where the model can be formulated as

$$\mathbf{y} = \mathbf{X}\beta \tag{2.6}$$

where $\mathbf{y}$ is the measurement (or response variable) vector, $\mathbf{X}$ is the regressor matrix and $\beta$ is the parameter vector. The objective function to be minimized in the OLS algorithm is the sum of squared residuals, that is written as

$$S(b) = (\mathbf{y} - \mathbf{X}b)^T(\mathbf{y} - \mathbf{X}b) \tag{2.7}$$

for a particular parameter vector $b$. The solution for the parameter vector $\beta$ that minimizes (2.7) can be obtained to be

$$\beta = (\mathbf{X}^T\mathbf{X})^{-1}\mathbf{X}^T\mathbf{y}. \tag{2.8}$$

The OLS algorithm with the sum of squared residuals objective function is sensitive to outliers in data. In order to reduce the effect of outliers, a robust least squares algorithm can also be used. The bisquare weights regression method, where a weighted sum of squares is minimized is also employed in this work through standard MATLAB commands.

## 2.6 Recursive Least Squares

The RLS filter is a recursive version of the least squares algorithm. It is used time and again through this work in different formulations because of its low memory requirements and computational simplicity. The Method section will elaborate further on specific formulations of the RLS filter for various scenarios.

The RLS filter is used to identify parameters in a linear regression model

$$y_k = \psi_{\mathbf{k}}^{\mathbf{T}}\theta_{\mathbf{k}} \tag{2.9}$$

where $y_k$ is the measurement, $\psi_{\mathbf{k}}^{\mathbf{T}}$ is the regression vector and $\theta_{\mathbf{k}}$ is the parameter vector at time instant k. The RLS with forgetting factor is highly suitable for adapting to time varying parameter vectors, and the cost function that is minimized by the optimum parameter estimates is an exponentially weighted linear least squares cost function

$$J = \sum_{s=1}^{k} \lambda^{k-s}(y_s - \hat{y}_s)^2 \tag{2.10}$$

where $y_s$ and $\hat{y}_s$ are the measurement and predicted measurement at time instant $s$ respectively. Error in the past samples are discounted through the use of the forgetting factor $\lambda$, which is usually set between 0.95 and 1. The parameter and covariance update equations that minimize the cost function described in (2.10) can be evaluated to be

$$\theta_{\mathbf{k}} = \theta_{\mathbf{k-1}} + \mathbf{P_k}\psi_{\mathbf{k}}(y_k - \psi_{\mathbf{k}}^{\mathbf{T}}\theta_{\mathbf{k-1}}) \tag{2.11a}$$

$$\mathbf{P_k} = \frac{1}{\lambda}\left(\mathbf{P_{k-1}} - \frac{\mathbf{P_{k-1}}\psi_{\mathbf{k}}\psi_{\mathbf{k}}^{\mathbf{T}}\mathbf{P_{k-1}}}{\lambda + \psi_{\mathbf{k}}^{\mathbf{T}}\mathbf{P_{k-1}}\psi_{\mathbf{k}}^{\mathbf{T}}}\right) \tag{2.11b}$$

The regressor vector is initialized to zero for negative indices, and the covariance matrix is initialized according to the expected error in parameters. The parameter vector can be initialized to an intelligent guess, and more detail on its choice will be discussed for specific problems.

## 2.7 Statistics

The arithmetic mean (simply referred to as mean) of N samples in a data set is the sum of all numbers divided by the number of elements in the dataset, expressed as

$$\overline{a} = \frac{1}{N}\sum_{k=1}^{N} a_k. \tag{2.12}$$

The standard deviation $\sigma$ of N samples in a data set is

$$\sigma = \sqrt{\frac{1}{N}\sum_{k=1}^{N}(a_k - \overline{a})^2}. \tag{2.13}$$

The standard deviation gives an impression of the extent of spread of data.

The z-score of a data point is the distance in terms of the number of standard deviations a data point is away from the sample mean. It can be represented as

$$z_k = \frac{a_k - A}{\sigma} \tag{2.14}$$

and gives a measure of how far away the point lies from the expected value.

The mean error, root mean square error and infinity norm ($\infty$ norm) are frequently used to measure the extent of error between the actual values ($y_k$) and an estimate ($\hat{y_k}$), and are described as

$$e_{mean} = \frac{1}{N}\sum_{k=1}^{N}(\hat{y_k} - y_k) \tag{2.15a}$$

$$e_{rms} = \sqrt{\frac{1}{N}\sum_{k=1}^{N}(\hat{y_k} - y_k)^2} \tag{2.15b}$$

$$||e||_\infty = max_k|\hat{y_k} - y_k| \tag{2.15c}$$

where $N$ is the number of measurement points.

## 2.8 Polynomial regression

In this work, the first degree polynomial $f(x) = mx + b$ is fit to the terminal voltage measurements to detect abnormal self-discharge. Although a MATLAB function is used to readily perform the fit, some principles of the fitting process are mentioned here. If the measurements are represented by $y_i$, $i$ being the time index, the regression attempts to minimize the sum of residual squares

$$RSS = \sum_{k=1}^{N} [y_k - f(x_k)]^2. \tag{2.16}$$

The solution for $m$ and $b$ that minimizes the RSS of (2.16) is given by

$$m = \frac{\sum_{k=0}^{N}(x_k - \bar{x})(y_k - \bar{y})}{\sum_{k=0}^{N}(x_k - \bar{x})^2} \tag{2.17}$$

$$b = \bar{y} - m\bar{x} \tag{2.18}$$

where $\bar{x}$ and $\bar{y}$ are the arithmetic mean of $x_i$ and $y_i$ respectively.

# 3

# Method

In this chapter, the implementation and methods used to perform simulations/estimation are presented.

## 3.1 Internal short circuit simulation

For design and evaluation of algorithms for fault detection, a simulation environment to mimic faults is needed. Here, various aspects involved in the implementation of fault simulation are described. A Simulink model of a battery pack consisting of 108 logical cells in series will first be used for fault simulation. Subsequently, a Simscape model of the battery pack shall be used in order to simulate faults on an individual cell in the logical cell unit to evaluate if the detection algorithms still function as expected.

### 3.1.1 Input current profiles

Various input current profiles will be used for evaluating fault detection algorithms. The well-known Artemis driving cycle is considered as the base current profile for algorithm testing. In Figure 3.1, one such testing current profile is shown, and it has been obtained by duplicating the base Artemis cycle. Furthermore, it is important to mention that the convention for current is positive for charging and negative for discharging.

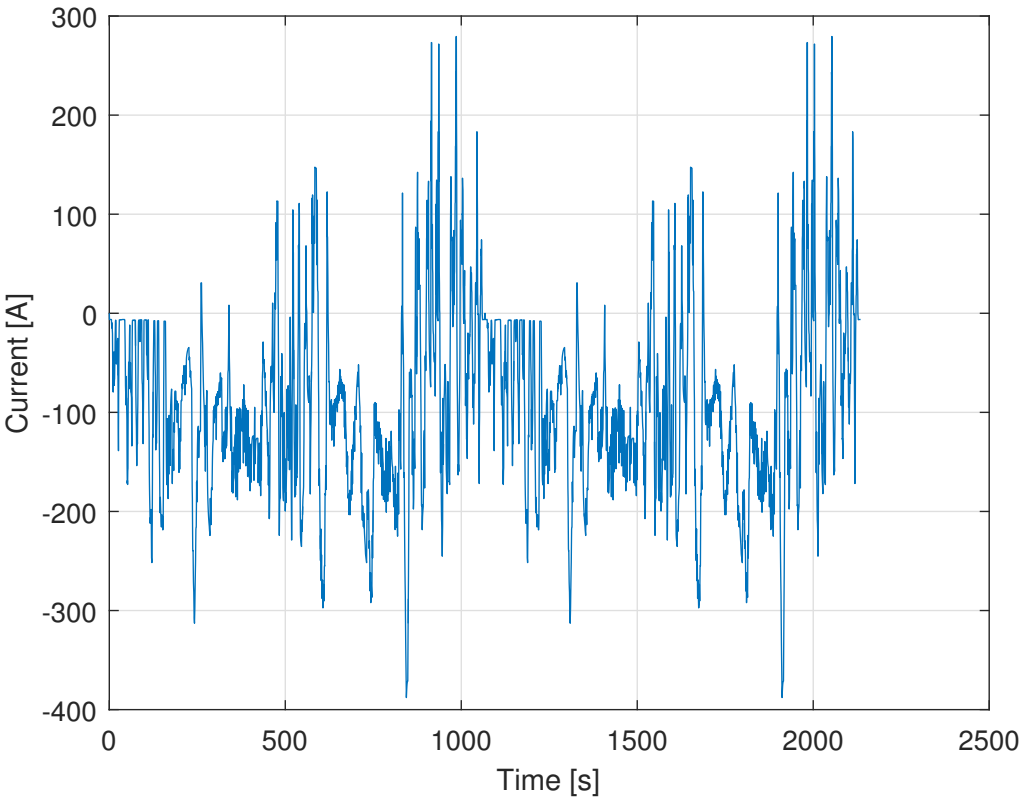


**Figure 3.1:** Artemis cell profile cycle

### 3.1.2 Implementation of ISCr model, Simulink

The MATLAB/Simulink model used for simulating a faulty logical cell unit is presented in this section. The entire logical cell is considered as a lumped individual cell and modeled as shown in Figure 3.2. The capacity of the logical cell is 180 Ah, and henceforth, for simplicity, the logical cell will be referred simply as a battery cell/cell in relation to the Simulink model. The implementation has been done along the same lines as (2.3), (2.4) and (2.5), with the voltage delay adjustment for avoiding the algebraic loop.

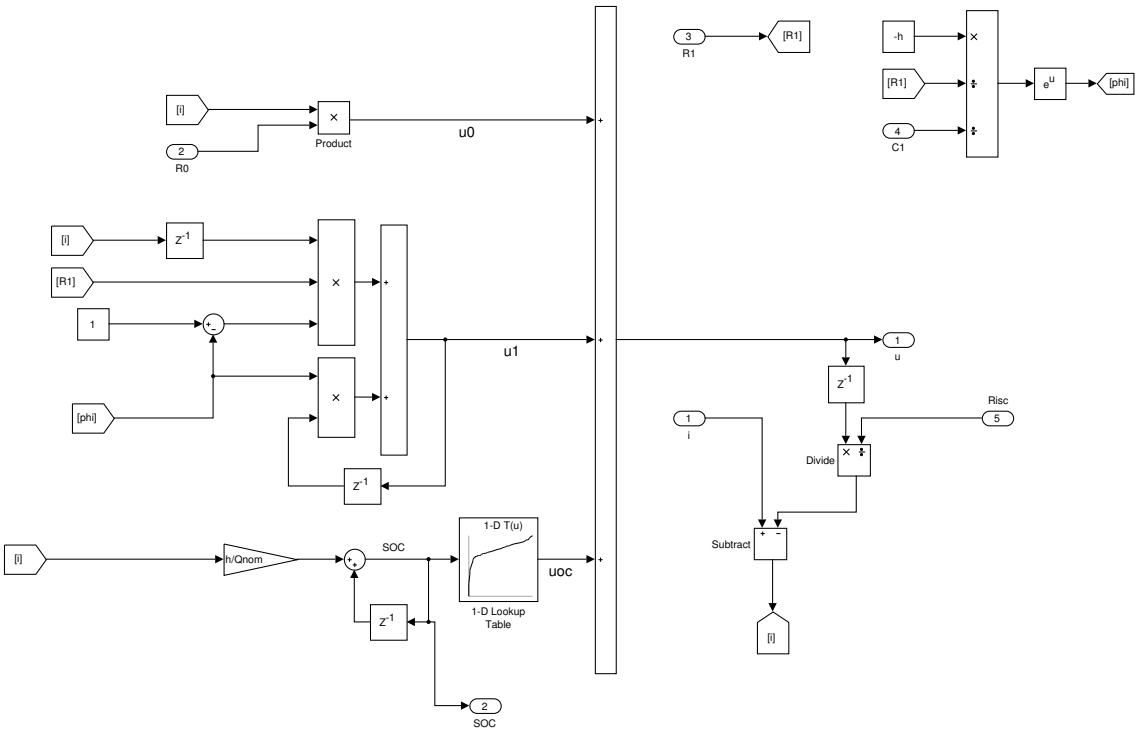


**Figure 3.2:** Faulty cell in Simulink

The three different voltage terms contributing to the terminal voltage in the first-order battery model are clearly displayed in Figure 3.2. Furthermore, the effects of an internal short circuit, modeled as an external resistance across the terminals of the battery is also shown. The values of $R_0$, $R_1$ and $C_1$ are obtained from external look-up tables and were derived from earlier characterization tests. They are expressed as a function of cell temperature, which is calculated for each cell as as a function of time in the overall battery pack model, and $SOC$. The $OCV$-$SOC$ relationship is also clearly seen as a look-up table in the model in Figure 3.2 and further seen in Figure 3.3. The initial $SOC$ is chosen to be 0.8 or 80% or these simulations and the sampling time for the simulations is obtained from the input current data.

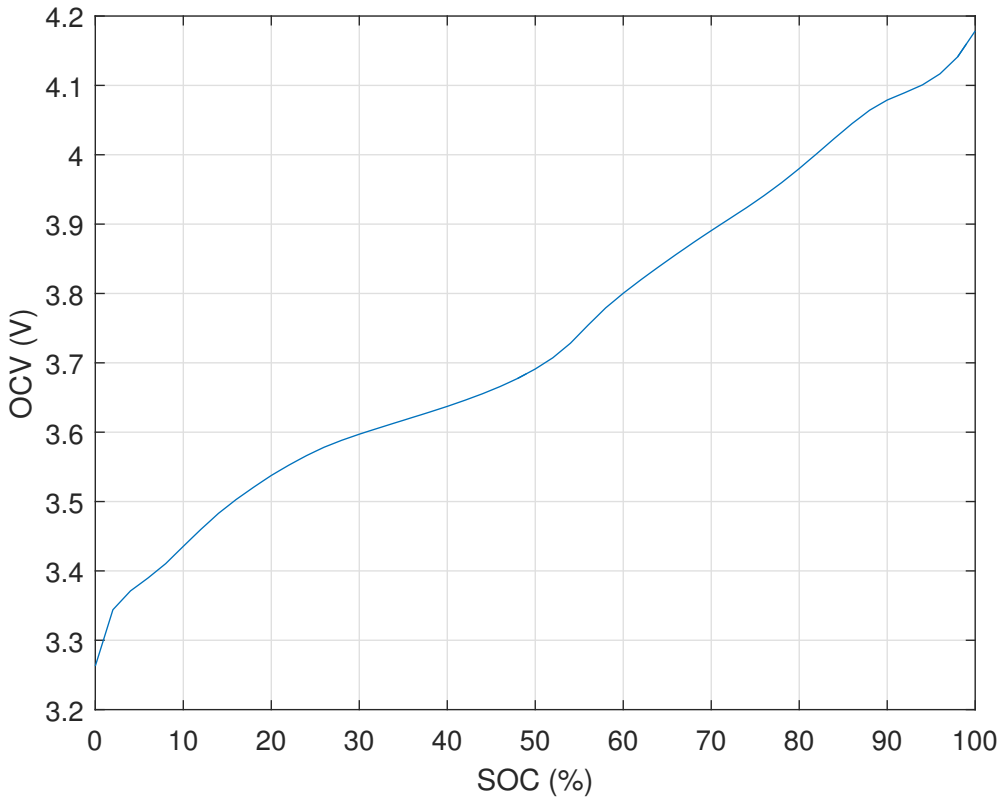


**Figure 3.3:** *OCV-SOC* curve of the battery cell

It is to be noted that the model shown in Figure 3.2 depicts a single cell belonging to a pack consisting of 108 cells in series. The fault can be triggered on any cell of choice at a pre-specified time in the battery pack after which the model shown in Figure 3.2 gets activated with the *Risc* input to initiate short circuit. It is important to note that the pack simulation also contains a thermal model to simulate cell temperatures that are then used in the electrical model to find values of various parameters. The temperature is computed using various parameters such as specific heat, density, volume etc employed in heat transfer equations. A detailed description and investigation of the thermal aspects is beyond the scope of this work.

Since the initial *SOC* specified for all cells is the same, the terminal voltage for all healthy cells throughout the driving cycle will be the same (albeit with small differences on account of different cell temperatures) and this is not so realistic. Thus, reasonable uncertainty is added to the voltage measurements to mimic a realistic scenario where voltages across cells have slight differences. The uncertainty is zero-mean and the standard deviation is obtained from experimental data.

### 3.1.3 Voltage measurement data uncertainties

In order to get an impression of the extent of variation of voltage measurements across the various cells (due to either/both differences in cell parameters or voltage

sensor errors), a previously obtained measurement data set for a battery pack is used. A particular time instant is chosen, and the deviation of each cell's voltage measurement from the mean voltage measurement (interpreted as error) is obtained and depicted in a histogram as shown in Figure 3.4.

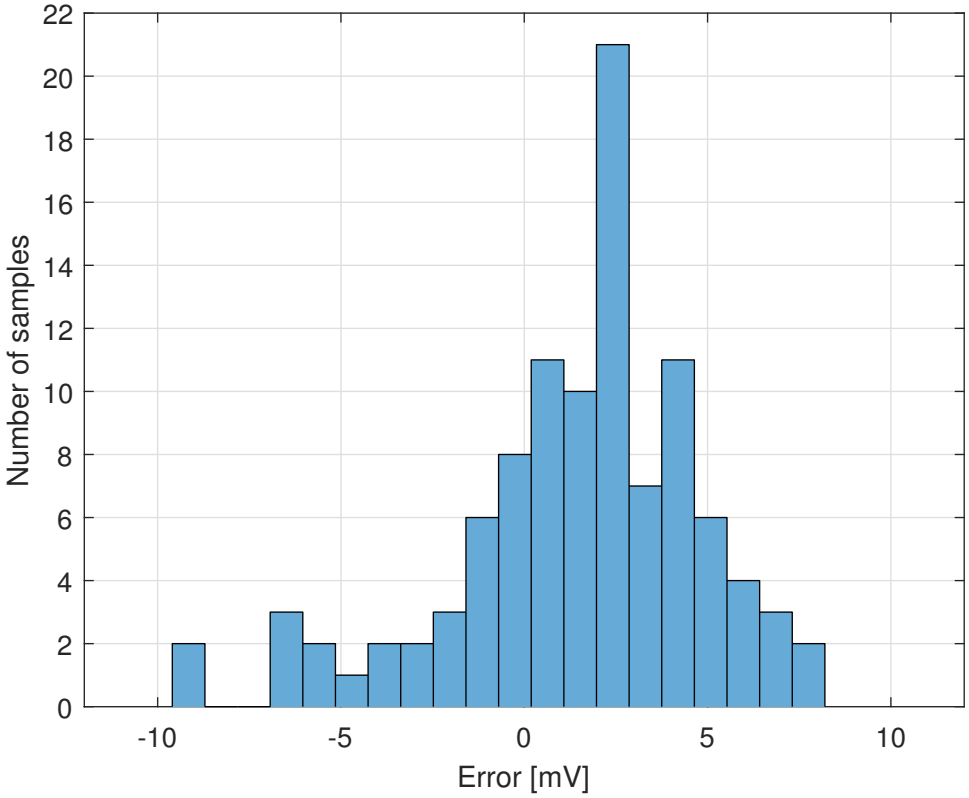


**Figure 3.4:** Voltage measurement 'error' histogram

As can be seen in Figure 3.4, the maximum deviation of a measurement from the mean value of voltage does not exceed ±10 mV. It is important to note that the mean value of the voltage measurement at the chosen time instant is 3.448 V and thus, the difference in measurements across voltage sensors is not very significant, with a maximum value of around 0.3 % deviation form the mean. This is because the cells and voltage sensors behave very similarly on account of consistency in both manufacturing and operating conditions. Furthermore, a number of other data points were checked and the deviation from mean does not exceed $\pm 10mV$.

The standard deviation of the voltage measurements from this chosen data set is evaluated and added to the voltage outputs from the simulation, under an of normal distribution. This results in a more realistic scenario where the voltage measurements used for the RLS algorithm are different for different cells. The standard deviation is obtained to be 3.4 mV, and the added noise is also zero mean, which is reasonable and can also be visually understood from Figure 3.4.

### 3.1.4 Fault simulations for various $R_{ISCr}$

Once the model for simulating the ISCr is developed, simulations are performed for various values of $R_{ISCr}$ and current profiles. The intention is to depict the change in the $SOC$ and $OCV$ for various intensities of short circuit conditions in the cell. Furthermore, the time at which the ISCr occurs can be varied, and this shall be utilized to observe trends in the estimated $OCV$.

The values of $R_{ISCr}$ considered for presenting effects of the short circuit are $1\Omega$ and $5\Omega$. The Simulink model with the faulty battery cell shown in Figure 3.2 is first used for simulation and detection of faults after which the Simscape model will be utilized.

## 3.2 Battery model in Simscape

In this section, the design of the battery model in Simscape will be described.

### 3.2.1 Component design

The battery pack model presented in Section 3.1.2 used a lumped model for the logical cells, and faults were also simulated on a chosen logical cell unit. It is important now to investigate the effects of a fault on an individual cell belonging to the logical cell unit, and check if the detection algorithms work satisfactorily.

In order to construct a logical cell in Simscape with three parallel cell units (described in Figure 2.1), the first step is to construct an individual cell. The component code is written for all units of the cell such as $OCV$, $R_0$, $R_1$ and $C_1$ and these blocks are then assembled together. One such example for the code written for the capacitance ($C_1$) block is shown below, and other components follow similar design methodology.

```
component C_1
% C_T
% Models a capacitor where the capacitance value (C) depends on an external
% physical signal inputs SOC and T. It is assumed that the capacitance
% value is slowly varying with time, and hence the equation i = C*dv/dt holds.

% Copyright 2012-2013 The MathWorks, Inc.

    nodes
        p = foundation.electrical.electrical; % +:left
        n = foundation.electrical.electrical; % -:right
    end

    inputs
        T = {293.15,'K'}; %T:left
```

```
    SOC = {1,'1'}; %SOC:left
end

parameters (Size=variable)
    C_Table    = {ones(5,3),'F'} % Vector of capacitance, C(SOC,T)
    SOC_Table = {[0;0.1;0.5;0.9;1],'1'} % State of charge(SOC) breakpoints
    Temp_Table = {[273.15 293.15 313.15],'K'} % Temperature(T) breakpoints
end

parameters
    v0 = {0,'V'}; % Initial voltage across capacitor
end

variables(Access=private)
    i = { 0, 'A' }; % Current
    v = { 0, 'V' }; % Voltage
end

function setup

    % Check parameter values
    if any(any(value(C_Table,'F')<=0))
        pm_error('simscape:GreaterThanZero','Capacitance values')
    end
    if any(value(Temp_Table,'K')<0)
        pm_error('simscape:GreaterThanOrEqualToZero','% Temperature');
    end

    % Set the initial voltage
    v = v0;

end

branches
    i : p.i -> n.i;
end

equations
    v == p.v - n.v;
    let
        % Perform the table lookup
        C = tablelookup(SOC_Table,Temp_Table,C_Table,SOC,T,...
            interpolation=linear,extrapolation=nearest)
    in
        % Electrical equation
        i == C * v.der;
```

```
        end
    end
end
```

The code above can be observed to have *nodes*, which describe the conserving ports of the block, i.e the positive and negative terminals in this case. *Inputs* are temperature (obtained from the thermal model) and $SOC$ (obtained from the $OCV$ component as an output) used to interpolate and calculate capacitance. *Parameters* can be specified in the block by the user and the *variables* are also mentioned as current and voltage in this case. It is noted that current is the through variable and voltage is the across variable. Finally, after a parameter validity check, the equations relating the variables and parameters are described to mathematically model the component. It is important to understand that the values of inputs and parameters seen in the code above are not actual values that shall be used in the calculations, but merely default values.

### 3.2.2 Battery cell in Simscape

Once all the components are designed, they can be interconnected to form a single battery cell as shown in Figure 3.5. The $OCV$, $R_0$, $R_1$ and $C_1$ components are observed clearly and are interconnected as in the Thevenin battery cell of Figure 2.1. It is important to mention here that the ECM parameters that were provided from the company are for a logical cell unit consisting of three individual cells in parallel. Therefore, in order to obtain parameters for an individual cell, assuming the cells are similar in nature and characteristics, the $R_0$ and $R_1$ parameters are scaled up by a factor of three and $C_1$ is scaled down by a factor of three. The capacity of the individual cells is obtained by dividing the capacity of the logical cell (180 Ah) by three. The power dissipation across the resistors is obtained as an output to use for the thermal model that simulates cell temperatures, and the $SOC$ and $OCV$ are also obtained as outputs to perform subsequent analyses. Simscape's physical modeling characteristic make it highly convenient for re-usability as shall be seen next in the creation of a parallel cell logical unit.

### 3.2.3 Logical cell for fault simulations

Once a cell is created in Simscape, three such units can be physically connected in parallel to form a logical cell unit shown in Figure 3.6, which will subsequently be used for fault simulation and testing. It can be seen that the interconnection is quite simple and also, the fault signals for each parallel cell are observed clearly. The purpose behind the use of a logical cell module to simulate faults is to investigate if a fault in one of the parallel cells in the module can still be detected by considering the logical cell as a lumped zeroth-order model. Since the proposed method involves comparative analysis, the notion of $SOC$ and $OCV$ for the lumped model can be used to evaluate if any of the logical cell modules deviates from the others

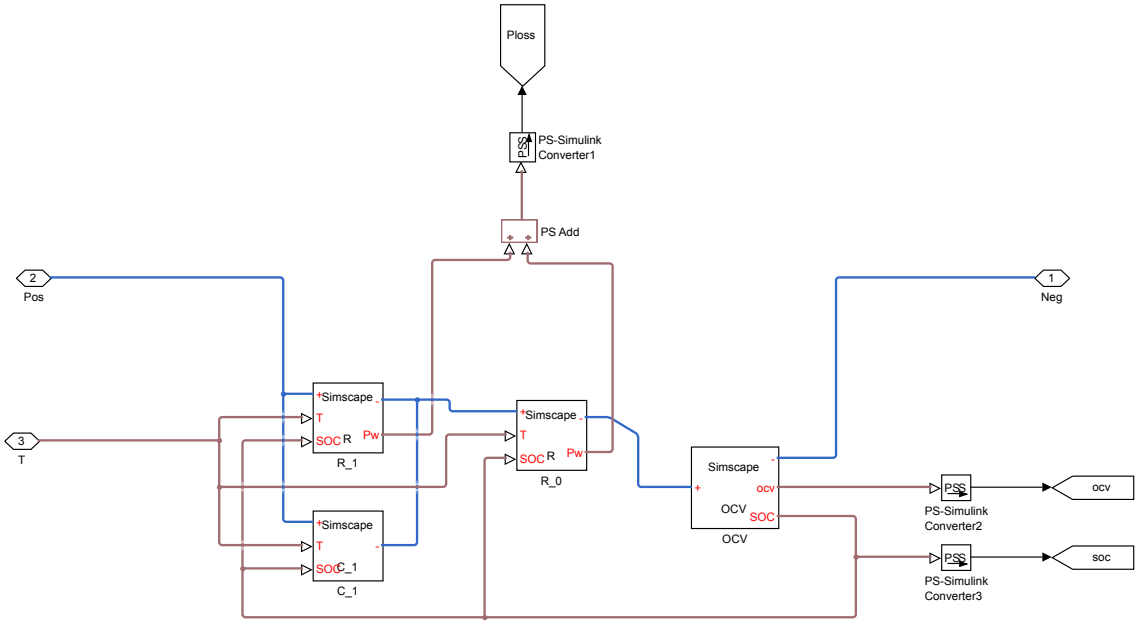


**Figure 3.5:** Battery cell in Simscape

significantly.

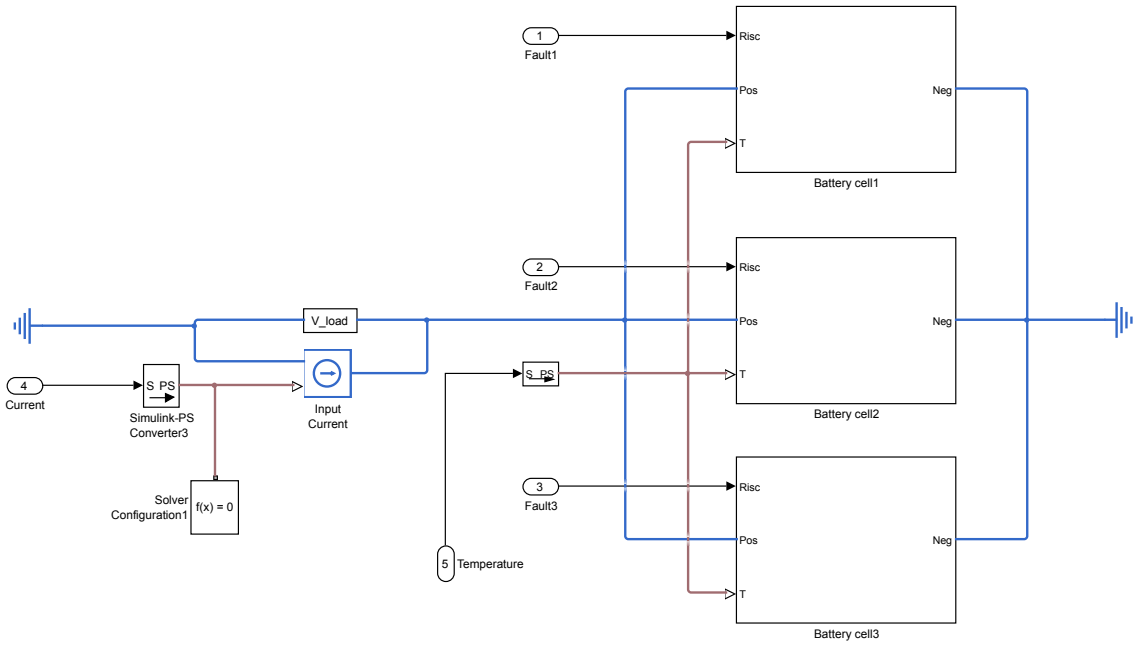


**Figure 3.6:** Battery logical cell in simscape

18 such logical cell units in series are considered for fault simulation and detection to save computation time without compromising on the comparative analysis. A fault is required to be simulated on one of the three parallel cells and then detected. However, if the same principle of simulating an internal short circuit using an external short circuit (connecting an $R_{ISCr}$ across the battery terminals) is followed, all cells

will be discharged equally due to the fact that they are in parallel and indistinguishable. Therefore, a slight modification is employed where the short circuit resistance is connected across just the $OCV$ branch of the faulted cell as shown in Figure 3.7 and not across the terminals. This is acceptable as the main aspect of simulating a fault is to ensure that the $SOC$ of the faulty cell drops faster than it would through just the load current. This can be ensured by the secondary discharge current that flows through $R_{ISCr}$ in Figure 3.7.

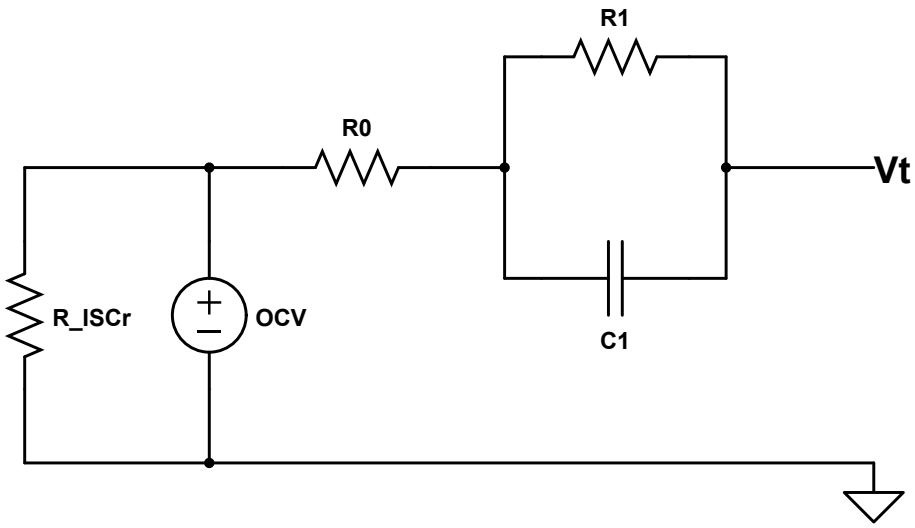


**Figure 3.7:** Faulted cell ECM used in Simscape

## 3.3 RLS for $OCV$ estimation

The RLS algorithm will be used to estimate the $OCV$ of the battery cell using the current and terminal voltage measurements. The equivalent circuit considered for the RLS estimation of $OCV$ will be a Rint model, which is a zeroth-order model with just an $OCV$ and internal resistance $R_0$ as depicted in Figure 3.8.

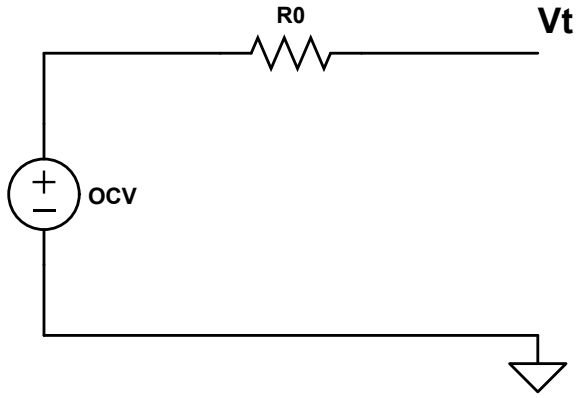


**Figure 3.8:** Battery Rint model

Note that the Rint model used for estimation of the $OCV$ is not the same as the Thevenin model used for simulation of the fault and thus, the $OCV$ estimation will

have some error as it will include the voltage drop across the polarization ($RC$) branch. However, as shall be seen later, the detection algorithm's performance is not affected as a consequence of thi inaccuracy. Furthermore, an RLS algorithm with a higher order model could be employed for more accurate estimation [32], but it can prove to be computationally more intensive, especially considering that a lower order model works satisfactorily.

The convention for current is taken as positive when charging and negative when discharging, and the equation for the terminal voltage is then

$$V(k) = U_{OC}(k) + I_L(k).R_0 \tag{3.1}$$

where $V(k)$ is the terminal voltage at time instant k, $U_{OC}(k)$ is the open circuit voltage at time instant k and $I_L(k)$ is the current at time instant k. $R_0$ is the internal resistance of the cell in the Rint model.

Equation 3.1 is now formulated to represent the regression vector $\psi_{\mathbf{k}}$, parameters $\theta_{\mathbf{k}}$ and output $y_k$ as

$$y_k = V(k) \tag{3.2a}$$

$$\psi_{\mathbf{k}} = \begin{bmatrix} 1 \\ I(k) \end{bmatrix} \tag{3.2b}$$

$$\theta_{\mathbf{k}} = \begin{bmatrix} U_{OC}(k) \\ R_0 \end{bmatrix} \tag{3.2c}$$

It is of importance to note that the parameter $R_0$ can also vary with time although it has not been explicitly mentioned in (3.1). The entities presented in (3.2) can be expressed in the form warranted for the RLS algorithm as $y_k = \psi_{\mathbf{k}}^{\mathbf{T}}\theta_{\mathbf{k}}$.

The initial values of the parameter vector and the error covariance matrix $\mathbf{P_0}$ are appropriately chosen as shall be described in the results. As far as the forgetting factor is concerned, there have suggestions for selecting an optimum value based on mathematical considerations [33] but in this work, a forgetting factor will be chosen through trial and error.

## 3.4 Moving window linear regression method for fault detection

In this section, the principles of using a moving window linear regression to detect faults that operate over longer time horizons will be discussed. The previously described method with the $OCV$ estimation can work satisfactorily for instantaneous faults, but slow degradation of a cell over the long term can be simply detected with a linear regression applied to moving time windows. The regression considered

will be a linear polynomial fit applied to a certain time horizon on all the terminal voltage measurements in that window. The slope of the line for a particular cell is a good indicator of the level of discharge in that cell, and consequently, if any of the slopes of the cells in the battery pack are higher than the others and get worse with time, abnormal self-discharge is detected.

A long driving profile is considered for simulating the terminal voltage in order to verify this method. This is accomplished by repeating the Artemis cycle with intermittent charging cycles to obtain a very long cycle that runs for a time of around 18 days. A small portion of this cycle (approximately 6 hours) is shown in Figure 3.9. it is important to mention that the Simulink model is used to simulate faults for this scenario as the purpose is to investigate the terminal voltage trend and not look at individual cell fault effects as dealt with in section 3.2.3.

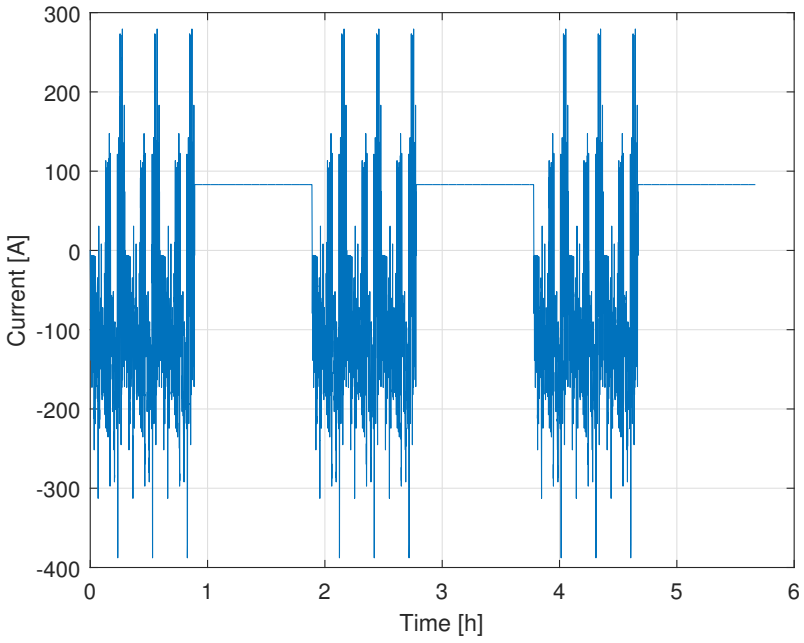


**Figure 3.9:** Long current profile used for fault detection

For a healthy cell, the current profile in Figure 3.9 results in the *SOC* and *OCV* profiles in Figure 3.10.

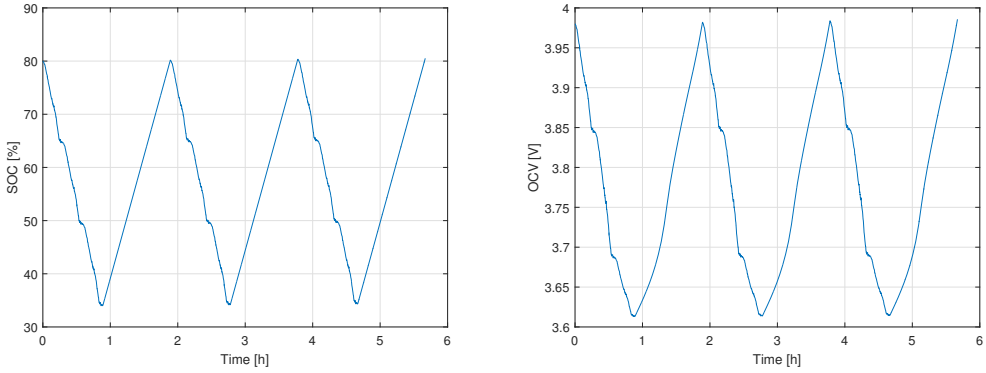


**Figure 3.10:** *SOC* and *OCV* of a healthy cell under the long driving cycle of Figure 3.9

The terminal voltage of the battery cell is essentially additional voltages (due to polarization and internal resistance for example) added to the open circuit voltage. Thus, if the *OCV* of one of the cells has a decreasing trend due to abnormal self-discharge over a long time frame, the terminal voltage also has a decreasing trend, which can be identified through a linear curve fit.

The magnitude of the $R_{ISCr}$ considered here is much larger as compared to the internal short simulation case, to simulate very low levels of self-discharge. A value of 50 Ω and 200 Ω will be considered to simulate different levels of abnormal-self discharge of one of the logical cells in a similar experimental set-up as in section 3.1.2. The *polyfit* function in MATLAB is utilized to perform linear curve fits on voltage measurements for a chosen time window of 2 days. It is important to note that other appropriate time windows can also be chosen through a more rigorous analysis using actual experimental data. As before, the experimentally obtained uncertainty on the voltage measurements are added to the simulated terminal voltage to mimic an actual scenario.

## 3.5 *SOC* and parameter estimation using a high pass filter

The parameter estimation procedure using a high pass filter will be described in this section. Once the *SOC* of the cell is estimated using this method, it can be used to estimate both capacity and $R_{ISCr}$ as shall be seen in the subsequent section.

Let us begin by forming the following pre-estimate of *SOC* using coulomb counting

$$\widehat{SOC}_{pre}(t) = \widehat{SOC}_0 + \frac{h}{\hat{Q}_{nom}} \int_0^t i(\tau) d\tau \tag{3.3}$$

where $h$ is the sample time, $\widehat{SOC}_0$ is the initial *SOC* and $\hat{Q}_{nom}$ is the assumed capacity. It can be seen immediately that errors in $\widehat{SOC}_{pre}(t)$ will be in the low frequency range, and could be a consequence of errors in $\widehat{SOC}_0$, $\hat{Q}_{nom}$ and current

sensor errors, the high frequencies of which are filtered out because of the integrator.

An estimate of $U_0 + U_1$, $\widehat{U}_{01}$ can then be formed as

$$\widehat{U}_{01}(t) = U(t) - focv(\widehat{SOC}_{pre}(t)) \tag{3.4}$$

where $U$ is the measured terminal voltage and $focv$ is the $SOC$-$OCV$ relationship. Further, $focv(\widehat{SOC}_{pre}(t))$ can be termed as $\widehat{OCV}_{pre}(t)$.

It is reasonable to assume that the signals $U_{01}$ and $U_0$ will be very close in magnitude for high frequencies. This is illustrated in Figure 3.11.

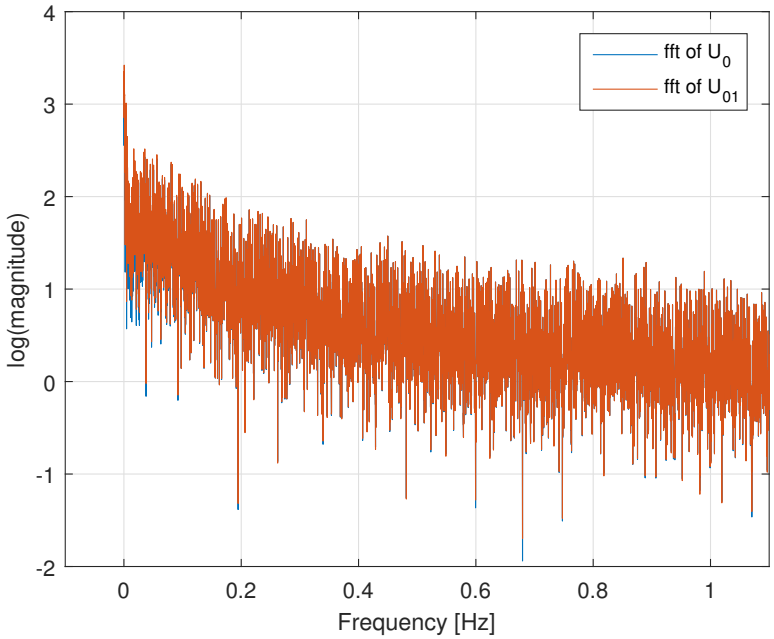


**Figure 3.11:** $U_{01}$ and $U_0$ frequency domain spectra

The reason why $U_{01}$ and $U_0$ behave in this manner is because the signal $U_1$ contained in $U_{01}$ is a low frequency signal due to the RC link acting as a low pass filter on the input current signal. On the other hand, the signal $U_0$ contains all the frequencies of the input current signal as it is merely a scaled version of the same by a factor of $R_0$. Thus, if a high pass filter $G_{HF}$ is used, $R_0$ can be estimated from the relation

$$G_{HF}\widehat{U}_{01}(t) = R_0 G_{HF} i(t) \tag{3.5}$$

on which an RLS filter can be employed to form the estimate $\widehat{R}_0$. It is important to mention though that the high-pass filter is not explicitly applied as depicted in (3.5) in the implementation. The difference operator, which is the counterpart of differentiation in the discrete time domain is instead used to amplify higher frequencies. The forgetting factor and initial covariance used for the RLS filter are chosen by trial and error and depicted in Table 3.1.

**Table 3.1:** Forgetting factor and initial covariance for $R_0$ RLS estimator

| Forgetting factor | Initial covariance |
|---|---|
| 0.995 | $2 \times 10^{-7}$ |

Once $\widehat{R}_0$ is obtained, $\widehat{U}_0(t)$ is calculated as $i(t)\widehat{R}_0$ and an initial estimate of $U_1$ ($\widehat{U}_{1_{pre}}$) can be then formed by simple subtraction as per

$$\widehat{U}_{1_{pre}}(t) = U(t) - \widehat{U}_0(t) - \widehat{OCV}_{pre}(t) \tag{3.6}$$

Again, since the errors in $\widehat{U}_{1_{pre}}$ are low frequency errors contained in $\widehat{OCV}_{pre}$, it is reasonable to assume

$$G_{HF}\widehat{U}_{1_{pre}}(t) \approx G_{HF}U_1(t) \tag{3.7}$$

which is further displayed in Figure 3.12. The actual capacity of the cell is 180 Ah and actual initial $SOC$ is 0.80.

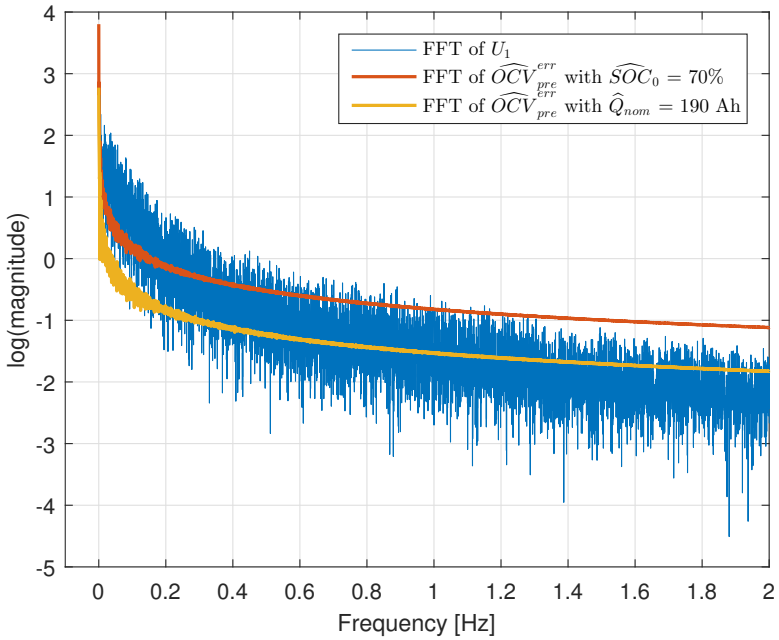


**Figure 3.12:** Frequency spectra of $U_1$ and $\widehat{OCV}_{pre}^{err}$ for $\widehat{SOC}_0 = 70$ % and $\widehat{Q}_{nom} = 190$ Ah

It is seen clearly that the 0 Hz component of $\widehat{OCV}_{pre}^{err}$ is high for both cases. However, $U_1$ dominates immediately after till about 0.6 Hz after which all signals become very low in magnitude.

As with $R_0$ estimation, the parameters $A$ and $B$ w.r.t the RC branch can be estimated using the high pass filtered signals of $\widehat{U}_{1_{pre}}(t)$ and $i(t)$ using an RLS filter applied to the relation

$$G_{HF}\widehat{U}_{1_{pre}}(t) = AG_{HF}\widehat{U}_{1_{pre}}(t-h) + BG_{HF}i(t-h) \tag{3.8}$$

expressed in the standard RLS formulation of $y_k = \psi_{\mathbf{k}}^{\mathbf{T}}\theta_{\mathbf{k}}$. The high pass filter used is a Butterworth filter with a cutoff frequency of 0.005 Hz. The filter order is chosen as 2. The IIR nature of the filter introduces distortions in the signals on account of its non-linear phase response, but this will not affect parameter estimation as it is applied to both the current and voltage signal as seen in (3.8). The forgetting factor for the RLS filter is chosen as 0.998 through trial and error. Furthermore, the initial covariance matrix $\mathbf{P}_0$ for the RLS filter is chosen as

$$\mathbf{P}_0 = \begin{bmatrix} 1000 & 0 \\ 0 & 0.0001 \end{bmatrix} \tag{3.9}$$

Once estimates $\widehat{A}$ and $\widehat{B}$ are formed, the estimate $\widehat{U}_1$ for all frequencies can be obtained using

$$\widehat{U}_1(t) = \widehat{A}\widehat{U}_1(t-h) + \widehat{B}i(t-h). \tag{3.10}$$

Finally, it is straightforward to obtain the final estimates of $OCV$ and $SOC$ using the relationships

$$\widehat{OCV}(t) = U(t) - \widehat{U}_0(t) - \widehat{U}_1(t) \tag{3.11a}$$

$$\widehat{SOC}(t) = focv^{-1}(\widehat{OCV}(t)) \tag{3.11b}$$

The entire parameter and $SOC$ estimation procedure is summarized in the flowchart of Figure 3.13.

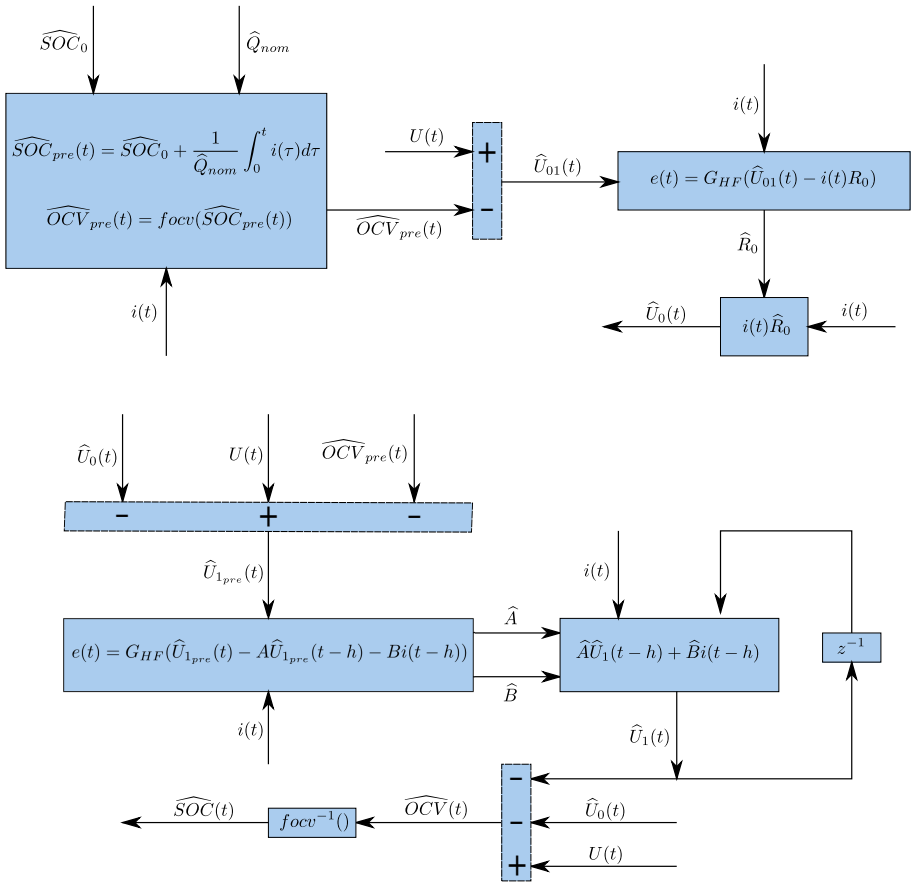


**Figure 3.13:** Process flow depicting $R_0$, $A$, $B$ and $SOC$ estimation. The two RLS filters are shown as blocks that minimize error $e(t)$

### 3.5.1 Problem with insufficient excitation

In the RC branch parameter estimation step, specific criteria with respect to high frequency content of the current signal must be met for update of the RLS filter. The condition can be described as

$$\sqrt{\frac{1}{T}\int_{t-T}^{t} |I_F^2| d\tau} > threshold \tag{3.12}$$

where $T$ is chosen to be 40 s and the *threshold* is chosen to be 30 A on the basis of trial and error. This update condition ensures reliable parameter estimation as the estimates may diverge in the presence of current and voltage sensor noises. In order to demonstrate this effect, a simulation only of the RC branch is considered and band limited white noise is added to the current and voltage signals. The estimation of parameters $A$ and $B$ is subsequently accomplished using the RLS filter without the update criteria of (3.12).

The noisy current signal ($I$), noisy voltage signal ($U_1$) and parameter estimates $A$ and $B$ are depicted in Figure 3.14.

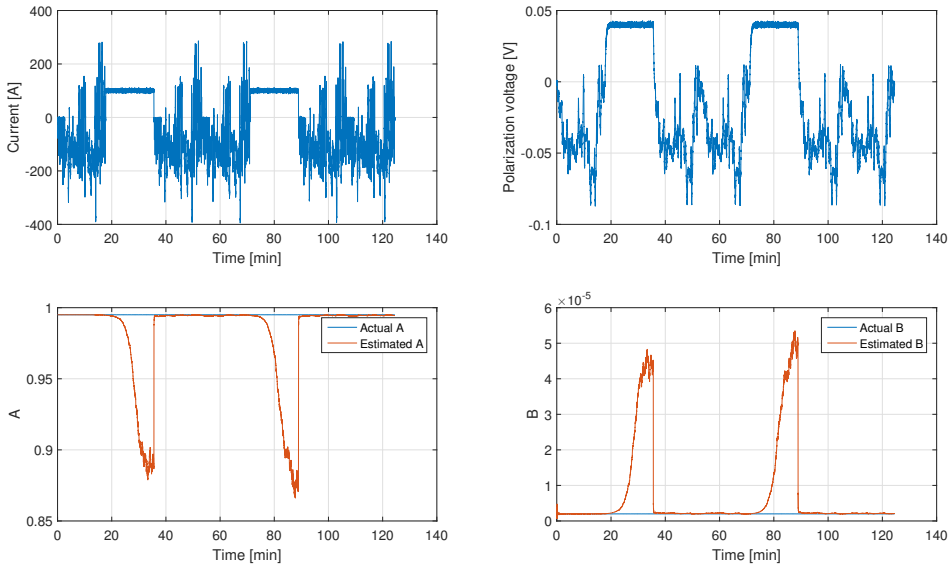


**Figure 3.14:** $A$ and $B$ estimation in the presence of sensor noises

It is seen clearly in Figure 3.14 that the parameter estimates diverge when current is constant. Therefore, an excitation condition is required to dictate the update stage of the RLS algorithm.

### 3.5.2 Modification of $R_0$ estimation

In section 3.5, it was mentioned that the estimation of $R_0$ can be accomplished using $G_{HF}\widehat{U}_{01}$ as it is approximately $G_{HF}\widehat{U}_0$. However, it was observed that $\widehat{R}_0$ had a bias with respect to the actual value $R_0$ using this method. This is because of $G_{HF}\widehat{U}_1$ is present as a disturbance in $G_{HF}\widehat{U}_{01}$, despite its relatively small magnitude.

In order to eliminate this disturbance, estimates $\widehat{A}$ and $\widehat{B}$ from the subsequent estimation stage are feedbacked through a low pass filter to the $R_0$ estimator. $G_{LF}\widehat{A}$ and $G_{LF}\widehat{B}$ are used to calculate an estimate of the polarization voltage $\widetilde{U}_1$, which is used to form an estimate $\widehat{U}_{0_{pre}}$ using the relation

$$\widehat{U}_{0_{pre}} = U(t) - \widehat{OCV}_{pre}(t) - \widetilde{U}_1(t). \tag{3.13}$$

The time constant of the low pass filter (used to ensure stability) is chosen to be the rise time of the responses of the $\widehat{A}$ estimator, approximately 50 s. The difference operator applied to $\widehat{U}_{0_{pre}}$ is then used to estimate $R_0$ instead of $\widehat{U}_{01}$.

## 3.6 Capacity $Q$ and $R_{ISCr}$ estimation using $\widehat{SOC}$ estimate

The estimate of the state of charge ($\widehat{SOC}$) formed using the method described in the previous section is used now to estimate capacity $Q$ and the short circuit resistance $R_{ISCr}$. The equation used for the estimation is formulated as

$$S\hat{O}C(k) = S\hat{O}C(0) + \frac{h}{Q}\sum_{n=0}^{k} I(n) - \frac{h}{Q.R_{ISCr}}\sum_{n=0}^{k} V(n) \tag{3.14}$$

where $I$ is the current, $V$ is the terminal voltage and $h$ is the sampling time. The least squares algorithm shall be used to estimate the parameters $\widehat{SOC}(0)$, $\frac{h}{Q}$ and $\frac{h}{Q.R_{ISCr}}$ using data over the entire driving profile. The measurement vector ($\mathbf{y}$), regressor matrix ($\mathbf{X}$) and parameter vector ($\beta$) are expressed as

$$\mathbf{y} = \begin{bmatrix} S\hat{O}C(0) \\ S\hat{O}C(1) \\ ... \\ S\hat{O}C(end) \end{bmatrix} \tag{3.15a}$$

$$\mathbf{X} = \begin{bmatrix} 1 & I(0) & V(0) \\ 1 & I(0)+I(1) & V(0)+V(1) \\ ... & ... & ... \\ 1 & \sum_{n=0}^{end} I(n) & \sum_{n=0}^{end} V(n) \end{bmatrix} \tag{3.15b}$$

$$\beta = \begin{bmatrix} S\hat{O}C(0) \\ \\ \frac{h}{Q} \\ \\ \frac{h}{Q.R_{ISCr}} \\ \\ \end{bmatrix} \tag{3.15c}$$

to form the LS model $\mathbf{y} = \mathbf{X}\beta$. The capacity estimate $\widehat{Q}$ and the short circuit resistance estimate $\widehat{R}_{ISCr}$ are then obtained from the estimate of parameter vector $\beta$.

The ordinary least squares estimator is sensitive to data outliers and hence, a robust least square estimator with a modified cost function will also be used to evaluate parameters $\widehat{Q}$ and $\widehat{R}_{ISCr}$. The formulation of the model remains the same as that depicted in (3.15).

# 4

# Results

In this section, results for the fault simulation models and detection algorithms are presented. Detection strategies that involve a comparative analysis without estimation of $R_{ISCr}$ are presented first. Subsequently, the high pass filter based $R_{ISCr}$ estimation procedure will be highlighted.

## 4.1 ISCr simulation with the Simulink model

Effects of an internal short circuit on $SOC$ is first evaluated for various $R_{ISCr}$. Figure 4.1 depicts the $SOC$ for all the 108 cells in the battery pack with an $R_{ISCr}$ of 5Ω on cell number 37 at 500 s.

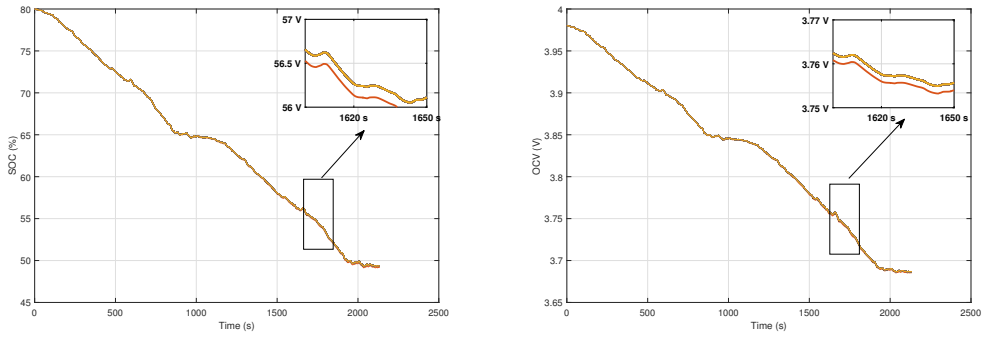


**Figure 4.1:** $SOC$ and $OCV$, $R_{ISCr}$ of 5 Ω

As can be seen in Figure 4.1, the $SOC$ all cells drop at the same rate until 500 s after which the faulted cell $SOC$ begins to deviate due to the internal short circuit. The $OCV$ of the cells depict a similar behaviour to the $SOC$ are also seen in Figure 4.1. It is clearly shown how small the deviation is for the faulty cell as compared with healthy cells, all of which follow the exact same profile (indicated by the yellow curve). To illustrate an example, the difference in $OCV$ of the faulted cell to the healthy cells is around 2 mV at 1700 s, or 0.05 %. This means that the 5 Ω internal short is not of extreme severity although, as shall be seen later, the RLS based detection method shows promising detection even with such a short. Furthermore, since the relationship between $SOC$ and $OCV$ is one to one, only the $OCV$ will be presented and discussed henceforth.

The deviation of the faulted cell $OCV$ is more pronounced for an $R_{ISCr}$ of 0.5 Ω as seen in Figure 4.2. This is expected as the value of $R_{ISCr}$ has been decreased by a factor of 10 as compared to Figure 4.1. The difference in $OCV$ at 1700 s between the faulty and healthy cells is 18 mV as compared to 3 mV for an $R_{ISCr}$ of 5 Ω.

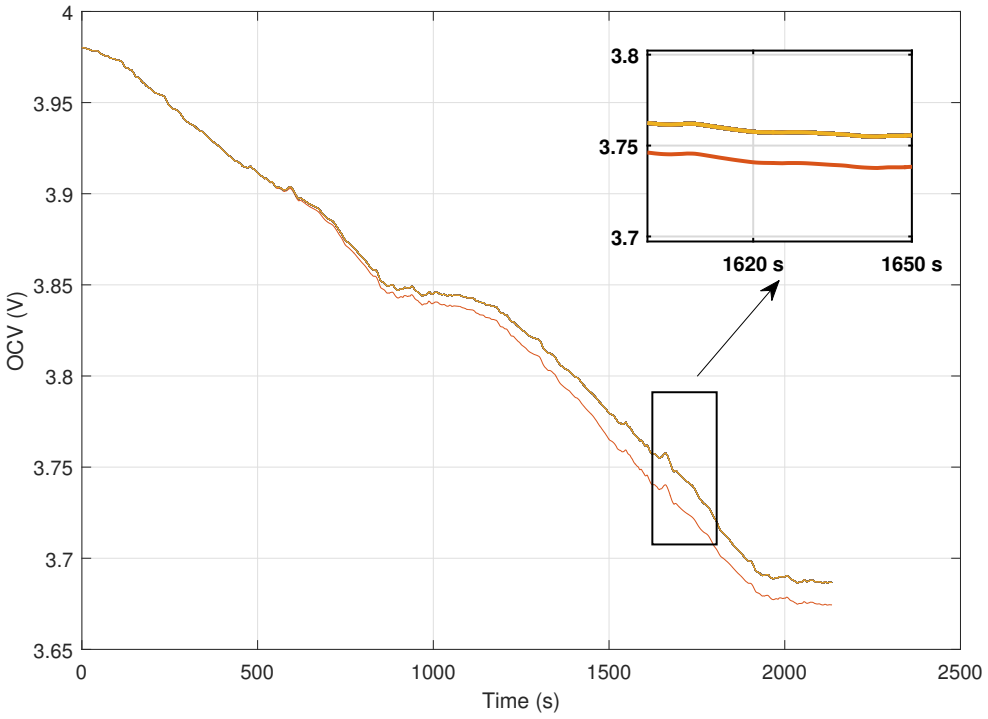


**Figure 4.2:** $OCV$, $R_{ISCr}$ of 0.5 Ω

As Figures 4.1 and 4.2 show, the effects of the short circuit on the $OCV$ increase as the value of $R_{ISCr}$ becomes smaller. This is further explained by the fact that the internal short is a secondary discharge mechanism in addition to the load current discharge, thereby depleting the $SOC$ of the battery to a greater extent than expected purely due to load current. This is also reflected in the $OCV$, and is the essence of the first detection method based on the Recursive Least Squares.

### 4.1.1 RLS based fault detection

In this section, the results of the RLS based fault detection strategy applied to the Simulink battery pack model will be discussed. The accuracy of the $OCV$ estimate of the faulty cell for different values values of $R_{ISCr}$ will be assessed and a comparative assessment of $OCV$s for different cells in the pack along the lines of [15] will be performed.

#### 4.1.1.1 Initialization and forgetting factor

Before proceeding with a description of the performance of the algorithm, the values chosen for initialization of the parameter vector shown in (3.2c) and the error covariance matrix for the RLS are ought to be mentioned. The initial value of the $OCV$ parameter is chosen to be the first value of the voltage measurement, while the initial value of $R_0$ is selected to be close to the expected value of the internal resistance, in the order of a few $m\Omega$ for the recursive estimation. It is to be noted that the algorithm performs satisfactorily even if a much higher value is chosen for $R_0$, if an appropriate initial error covariance is specified. In case the order of magnitude of $R_0$ is uncertain, a high value must be chosen for the initial variance for this parameter to ensure faster convergence to the right value. Since the confidence in the initial values of the parameters is reasonable in this project work, an initial variance of 0.1 is chosen for the $OCV$ parameter, and $10^{-4}$ for the $R_0$ parameter through trial and error. The covariance is chosen to be 0 assuming the parameters are uncorrelated.

#### 4.1.1.2 $R_{ISCr}$ of 1 Ω

The first case is investigated for an $R_{ISCr}$ of 1 Ω, which can be considered a short-circuit of moderate severity. The reason why this is considered a case of moderate severity is because the internal cell resistance is of the order of 0.3-0.4 $m\Omega$ which is much smaller than 1 Ω, and also because the load current magnitude of around 100 A is quite high compared to the short circuit current which is in the order of 3-4 A. The terminal voltage data for various cells are acquired from the battery pack simulation and appropriate error is added to these values to obtain a realistic scenario as described in section 3.1.3. The values thus obtained are considered to be the measurements for the RLS algorithm to function.

Figure 4.3 depicts the actual and estimated $OCV$ for the faulty cell with the Artemis current profile as input to the Simulink model.

It can be observed in Figure 4.3 that the estimated $OCV$ is quite close to the actual $OCV$. Upon closer examination, it can be seen that the $OCV$ estimate is lower than the $OCV$ for most part of the cycle. This is because the RLS uses a linear regression form based on a zeroth-order model while the simulation data is obtained from a first-order model. Hence, the $OCV$ estimate includes a part of the polarization voltage in addition to just the $OCV$ (the polarization voltage is negative during discharge due to the chosen convention).

The $OCV$ estimates for all the cells in the battery pack are illustrated in Figure 4.4.

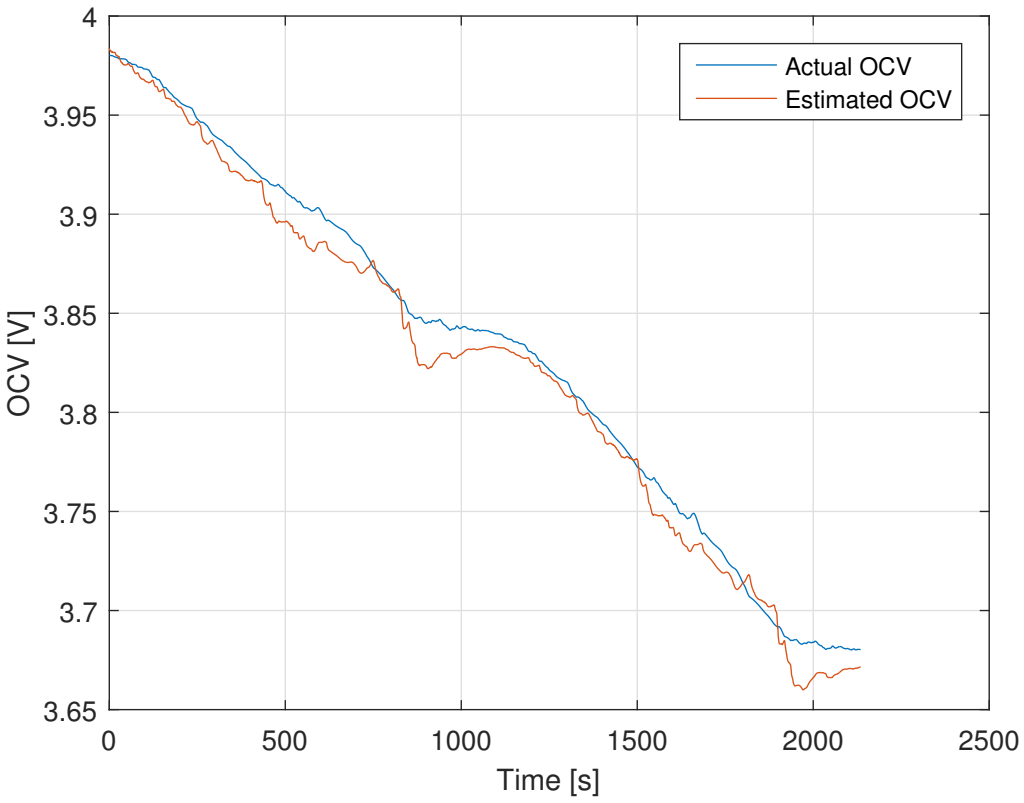


**Figure 4.3:** Actual and estimated $OCV$ of fault cell, $R_{ISCr}$ of 1 Ω

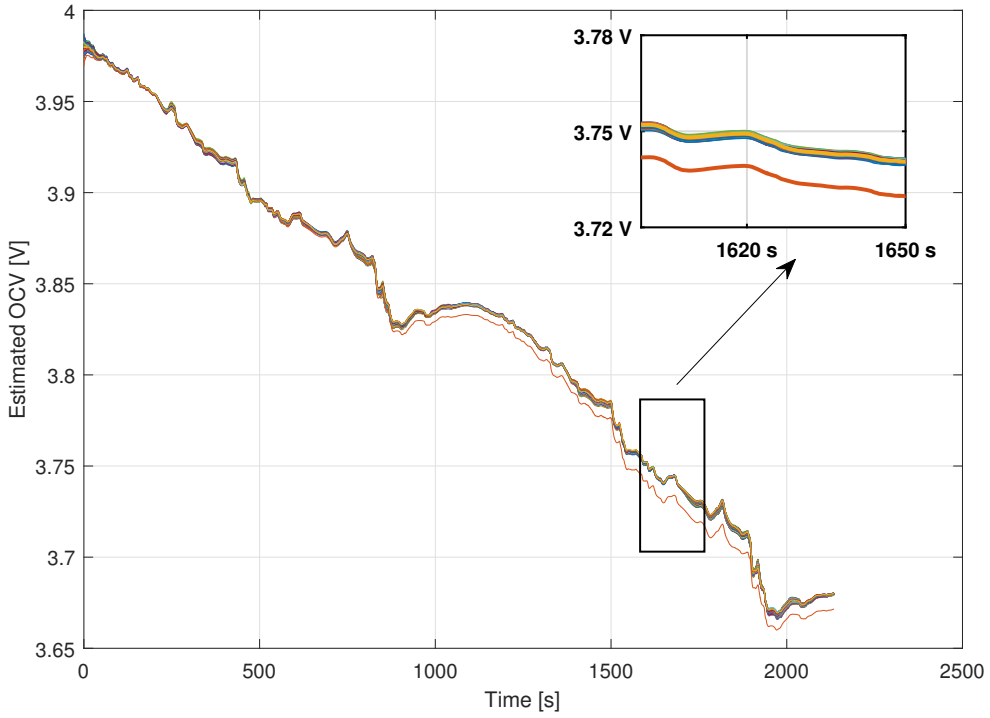


**Figure 4.4:** Estimated $OCV$ all cells, $R_{ISCr}$ of 1 Ω

It is observed from Figure 4.4 that one of the $OCV$ estimates begins to drift around 500 s upon application of the fault and it is precisely the $OCV$ estimate of the faulted cell. The deviation seems to become more pronounced as time progresses and is of similar nature as the behavior seen in Figure 4.2 of the actual $OCV$. Furthermore, the estimated $OCV$s of the healthy cells also seem to posses minor variations, a phenomenon that was absent in Figure 4.2 where the actual $OCV$s of healthy cells were observed to be the same. These variations occur because the thermal model employed in the battery pack considers heat flow across cells for temperature calculations, resulting in slightly different temperatures for various cells. This is seen in Figure 4.5 for 3 healthy cells at different positions in the battery pack. These temperature changes result in parameter variations in the ECM used in the simulation model that subsequently cause differences in the terminal voltage. This leads to the minor variations in the $OCV$ estimates for healthy cells which were observed in Figure 4.4.

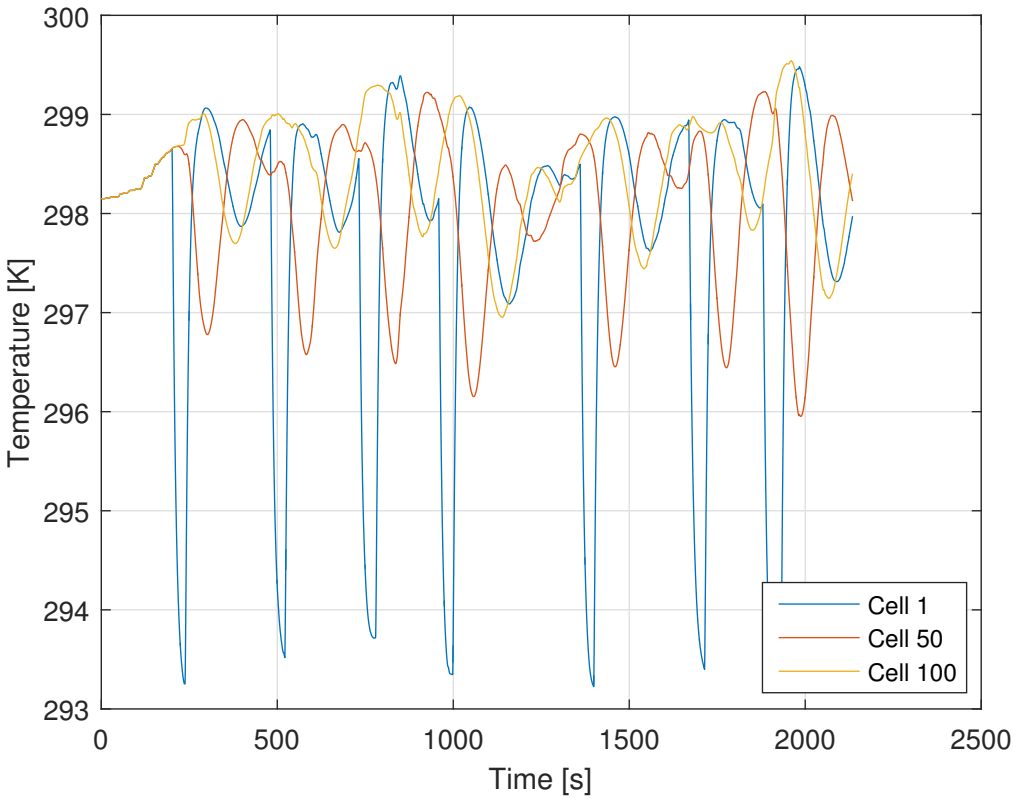


**Figure 4.5:** Temperature variation vs time for 3 chosen healthy cells

Various metrics showcasing the $OCV$ estimation error for the faulty cell are compiled are presented in Table 4.1.

**Table 4.1:** Faulted cell *OCV* error statistics

| Driving profile | mean error (mV) | RMSE (mV) | $\infty$ norm (mV) of |
|---|---|---|---|
| Artemis | -8.6 mV | 10.9 mV | 24.4 mV |

Having presented the *OCV* estimation results, a comparative analysis of the *OCV* estimates can be performed to identify faults. At every time instant, the z-score of all the *OCV* estimates is evaluated and if any of the *OCV* estimates are observed to deviate significantly, outside the $\pm 3\sigma$ limit for a significant period of time, a fault can be detected. Figure 4.6 depicts the z-scores vs time for the *OCV* estimates for all the 108 cells vs time with the $\pm 3\sigma$ limits.

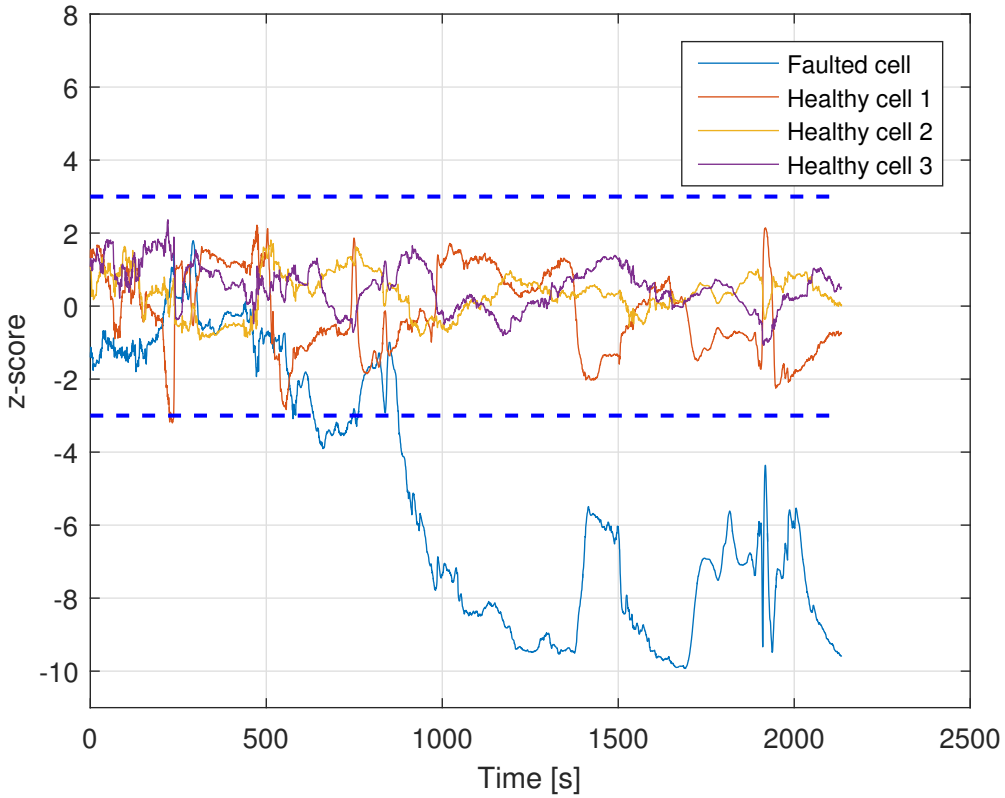


**Figure 4.6:** Z-scores vs time, *OCV* estimates

As can be seen in Figure 4.6, the z-score for the faulty cell drifts significantly outside the $-3$ limit soon after the fault at 500 s while the z-scores for the other cells stay within $\pm 2$. A detection strategy could be to check if the z-score for an *OCV* estimate strays outside the $\pm 4$ limit for more than a stipulated period of time, say 4 minutes, or to keep track of the proportion of time for which an *OCV* estimate strays outside the $\pm 3\sigma$ limit.

#### 4.1.1.3 $R_{ISCr}$ of 5 Ω

A similar performance evaluation is now presented for an $R_{ISCr}$ of 5 Ω. The actual and estimated $OCV$ plots are not presented for this case, but the metrics depicting the extent of error in the $OCV$ estimate in the faulty cell are presented in Table 4.2.

**Table 4.2:** Faulted cell $OCV$ error statistics

| Driving profile | mean error (mV) | RMSE (mV) | $\infty$ norm (mV) of |
|---|---|---|---|
| Artemis | -8.6 mV | 10.9 mV | 24.4 mV |

The z-scores of the $OCV$ estimates are presented in Figure 4.7.

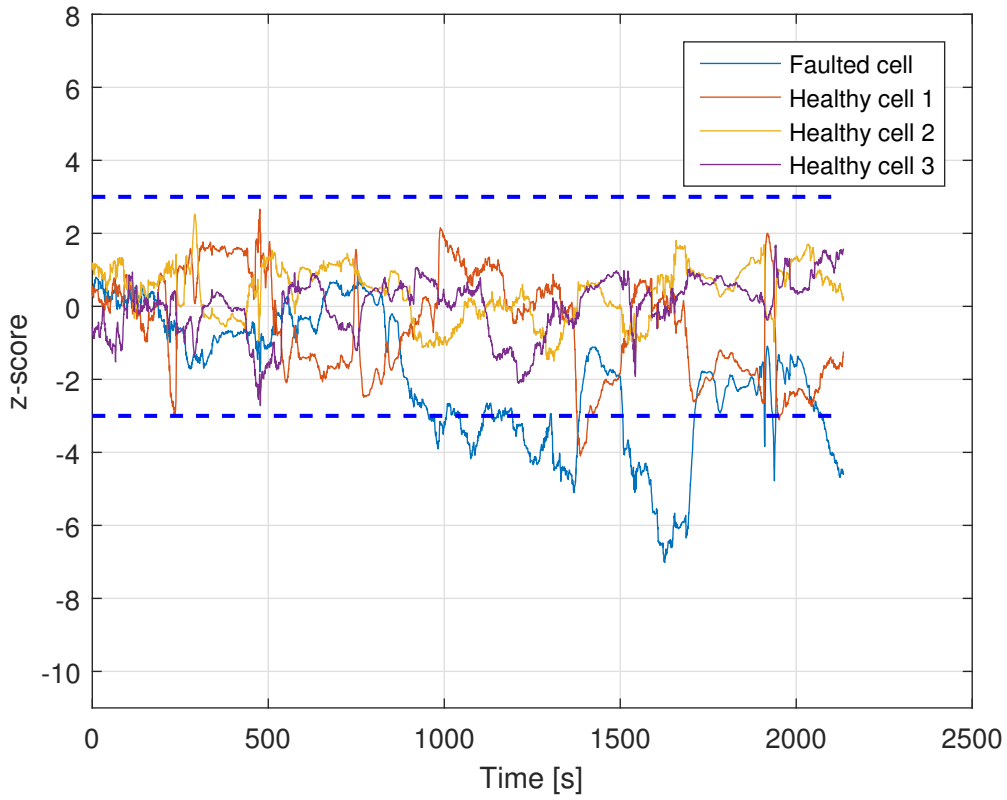


**Figure 4.7:** Z-scores vs time, $OCV$ estimates for 5 Ω $R_{ISCr}$

It is observed that the z-score for the faulty cell $OCV$ does not deviate out of the $-3$ limit as clearly as it did with a 1 Ω ISCr as was seen in Figure 4.6, but still strays outside of it for a significant proportion of time.

#### 4.1.1.4 Decaying $R_{ISCr}$

Now that the RLS filter based detection has been verified with the fault induced instantaneously at a certain time instant, the effects of a slowly degrading (decreasing) $R_{ISCr}$ is investigated. Furthermore, a much longer driving cycle will be used

for this case. The total length of the cycle is around 6 hours, and the faulty cell short-circuit resistance decays slowly from 11 Ω to a value less than 1 Ω at the end of the cycle. Figure 4.8 depicts the decaying $R_{ISCr}$ of the faulted cell and the z-scores based detection.

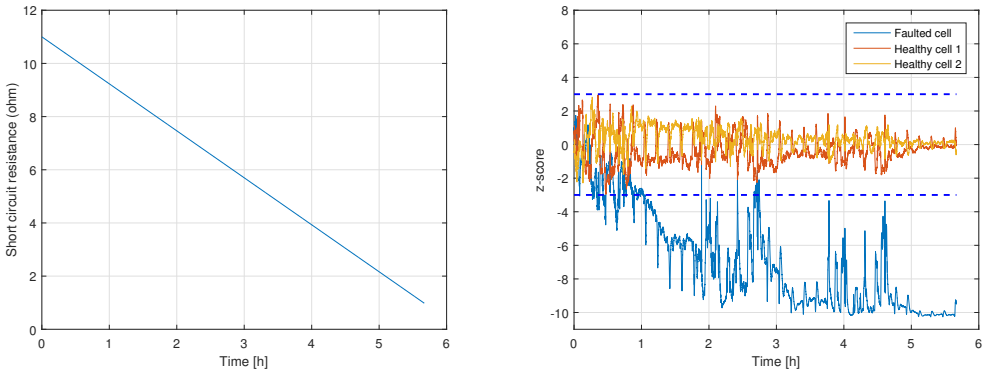


**Figure 4.8:** Faulted cell $R_{ISCr}$ and Z-scores based detection

It is seen clearly from Figure 4.8 that the z-score of the faulted cell deviates outside the -3 $\sigma$ limit around the 1 hour mark, when the short circuit resistance is 9 Ω. Thus, very early detection is possible in this case before the short circuit resistance drops further.

## 4.2 Simscape modeling and fault simulation

Now that the RLS filter based detection has been demonstrated for the Simulink model, investigations will be performed for faults in the Simscape model of a battery pack. As mentioned in section 3.2.3, three parallel individual cells are considered as a logical cell unit in a battery pack with 108 logical cells and a fault is induced on the first individual cell in logical cell number 37 at 500 s. For a value of $R_{ISCr}$ of 1 Ω, the $OCV$s of the three cells in the logical cell unit with the fault are presented in Figure 4.9. The $SOC$ of a healthy individual cell from another logical cell unit is also presented for reference. The individual cells in logical cell 37 are denoted by 37,1; 37,2 and 37,3.

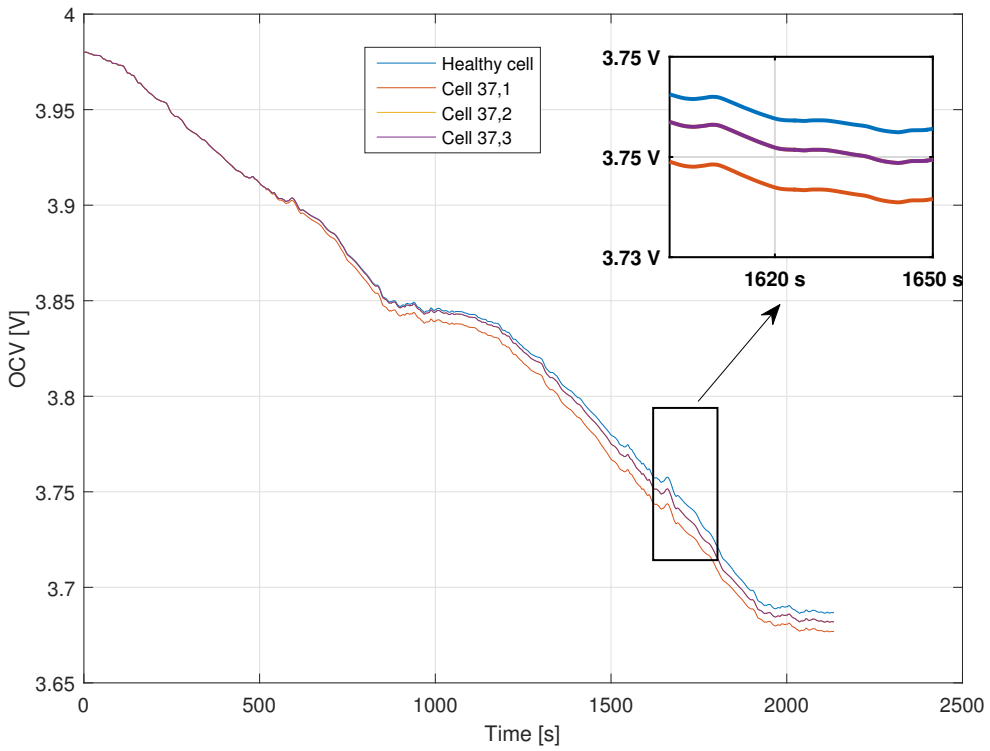


**Figure 4.9:** *OCV*s of various individual cells

As can be observed in Figure 4.9, the *OCV*s of the individual cells in logical cell 37 all decay faster than the healthy cell which is due to the fault. However, within the cells of logical cell 37, the first cell *OCV* decays faster than 2 and 3 (which are identical), as the fault is simulated only on the first individual cell according to the method in section 3.2.3. This achieves the desired effect of a fault on one of the individual cells in a logical cell block. The performance of the detection algorithm will be checked for different values of $R_{ISCr}$ applied to cell 37,1.

### 4.2.1 RLS fault detection

The *OCV* of a logical cell is estimated using the RLS filter as a lumped parameter, following which a comparative analysis is performed on similar lines as before with the z-scores. As before, uncertainties are added to the voltage measurements from the simulation to capture the combined effects of minor differences between cell characteristics and voltage sensor errors.

In Figure 4.10, the z-scores based detection is presented for faults of 1 Ω and 5 Ω. The actual and estimated *OCV* plots will not be presented since they look very similar to Figures 4.3 and 4.4.

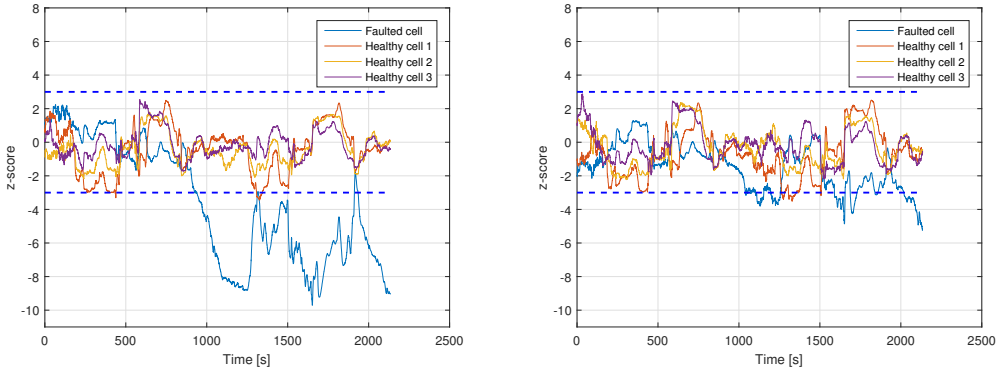


**Figure 4.10:** Z-scores based detection for $R_{ISCr}$ of 1 Ω and 5 Ω, Simscape model

It is seen that the detection algorithm performs satisfactorily for an $R_{ISCr}$ of 1 Ω on cell 37,1. However, the performance of the algorithm for an $R_{ISCr}$ of 5 Ω is not as conclusive as observed in Figure 4.7. This indicates that although an instantaneous fault on an individual cell can be detected using this method, the detection is conclusive for smaller values of the short circuit resistance.

## 4.3 Fault detection with a linear regression

In this section, the results of the moving window regression technique for detecting abnormal self-discharge is evaluated. A presentation of the effect of a minor abnormal self-discharge on both the *SOC* and *OCV* will first be presented after which results for the linear curve fit to identify abnormal self discharge are discussed.

As mentioned in section 3.4, a driving profile that is approximately 10 days long is considered, with a fault introduced on one of the cells. In order to highlight the motivation behind this method to detect abnormal-self discharge, the difference of the *SOC* and *OCV* between a healthy cell and the faulty cell, for a small period of 6 hours, is illustrated in Figure 4.11 for the 50 Ω $R_{ISCr}$.

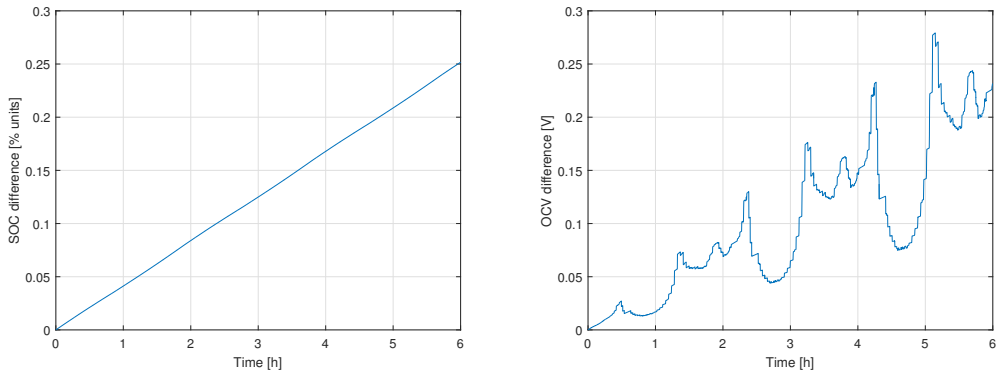


**Figure 4.11:** Difference in *SOC* and *OCV* between healthy and faulty cell

Figure 4.11 clearly depicts how the difference in *SOC* rises steadily with time. The

$OCV$ also shows an increasing trend but has peaks and valleys, which is because the $OCV$-$SOC$ relationship is not perfectly linear for all $SOC$ levels as seen in Figure 3.3. This increasing trend, over an appropriately long period of time, can be captured by a linear curve fit on the terminal voltages. A time window of 2 days is chosen to perform the linear curve fit. Figure 4.12 depicts the terminal voltage measurements and linear fits over a period of 4 days for the 50 Ω short, and just the voltage fits for the 200 Ω short for a period of 10 days.

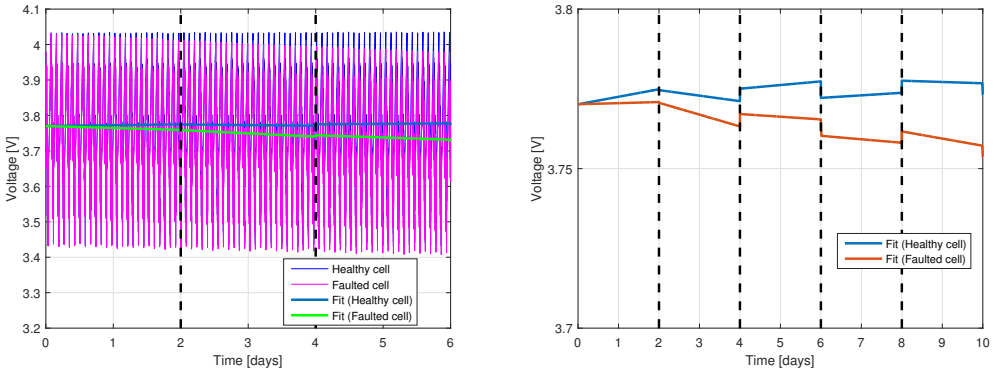


**Figure 4.12:** Terminal voltage measurements and linear fits, for shorts of 50 Ω and 200 Ω

As observed in Figure 4.12, the linear fit for the faulty cell exhibits a higher slope than the fits for a healthy cell and as the faulty cell degrades over time, the offset increases.

## 4.4 $SOC$ and parameter estimation using frequency separation

In this section, the $SOC$ and parameter estimation method using the high pass filter to remove low frequency errors is evaluated. Figure 4.13 depicts the estimation results without employing the high pass filter. An initial $SOC$ of 0.82 and capacity of 190 Ah is used in the estimation process. It is mentioned again that the actual initial $SOC$ is 0.8 and the capacity is 180 Ah in the plant model. The reference values for the parameters have steps of 10% for $R_0$ at 60 min and 1% for A at 40 min, both of which also leads to steps in the B reference used in the plant. Furthermore, the initial errors in $\widehat{R}_0$ and $\widehat{A}$ are +0.5% and -5% respectively.

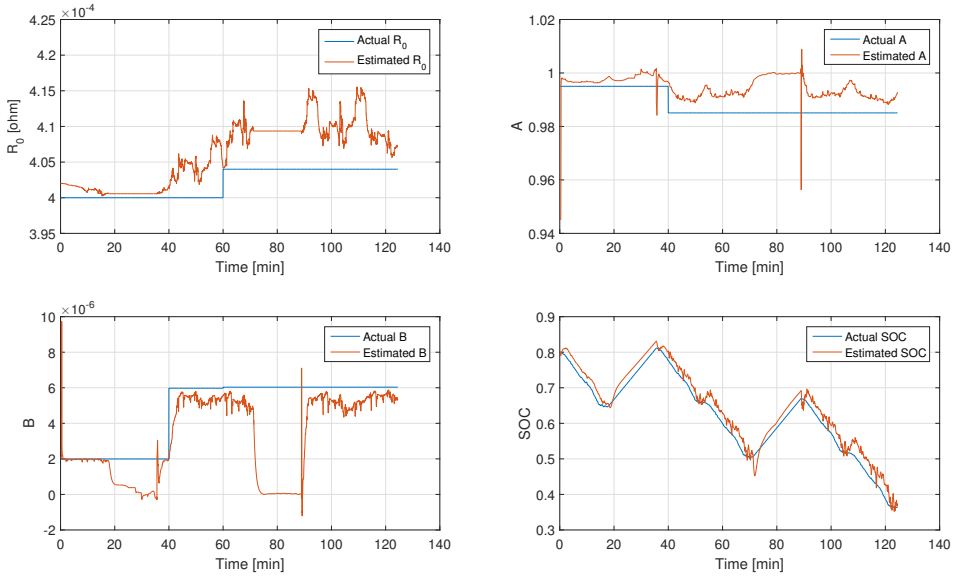


**Figure 4.13:** Parameter and $SOC$ estimates for a $\widehat{SOC}_0$ of 0.82 and $\hat{Q}_{nom}$ of 190 Ah

As can be seen in Figure 4.13, the estimates of the parameters and the $SOC$ do not converge satisfactorily to true values. This is because the incorrect initial $SOC$ ($\widehat{SOC}_0$) and $\hat{Q}_{nom}$ specified in the estimator propagate as low frequency errors to the parameter estimates and finally to the $SOC$ estimate.

In case $\widehat{SOC}_0$ is further away from the actual value of 0.8, say 0.7, the $SOC$ estimate actually diverges in intervals where $\hat{A}$ takes a value greater than 1 as seen in Figure 4.14.

The divergence can be explained by the fact that $\hat{A}$ is the pole of the RC-circuit, which is unstable for $A > 1$. This example shows the effects of low frequency errors over the final $SOC$ estimate, which will subsequently be used for capacity $Q$ and short circuit resistance $R_{ISCr}$ estimation.

The estimates are now presented after application of the high pass filter with a $\widehat{SOC}_0$ of 0.82 in Figure 4.15 and 0.7 in Figure 4.16.

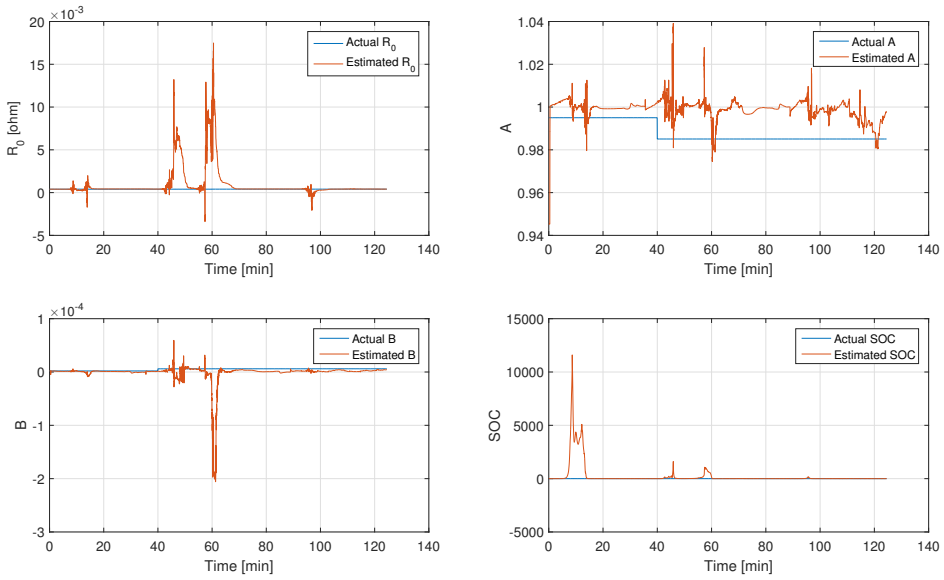


**Figure 4.14:** Parameter and $SOC$ estimates for a $\widehat{SOC}_0$ of 0.7 and $\widehat{Q}_{nom}$ of 190 Ah

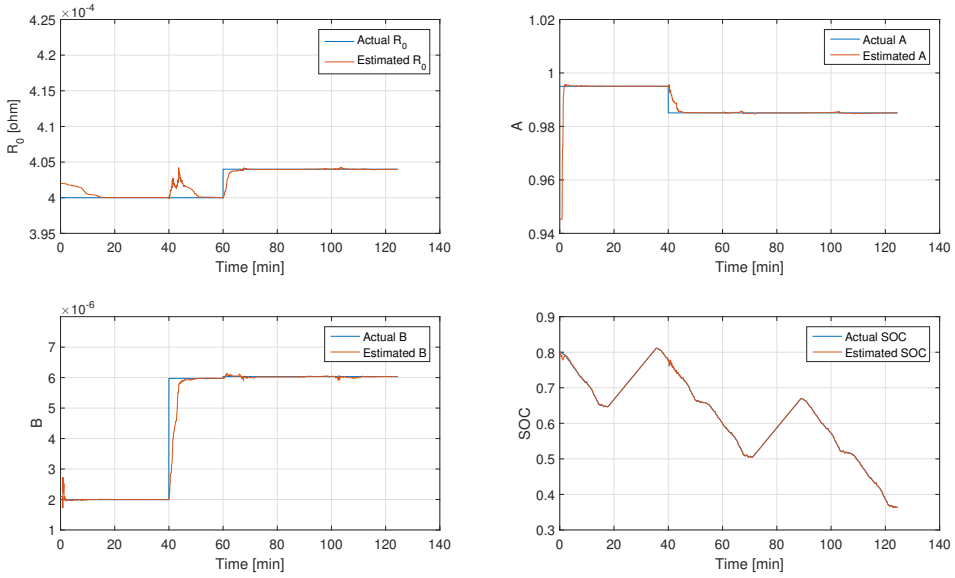


**Figure 4.15:** Parameter and $SOC$ estimates for a $\widehat{SOC}_0$ of 0.82 and $\widehat{Q}_{nom}$ of 190 Ah using a high pass filter

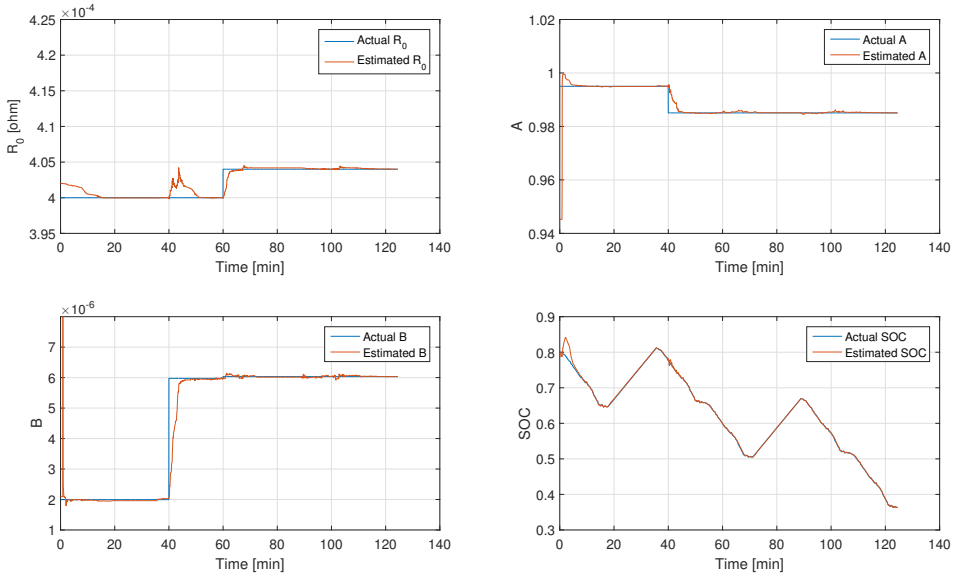


**Figure 4.16:** Parameter and $SOC$ estimates for a $\widehat{SOC}_0$ of 0.7 and $\widehat{Q}_{nom}$ of 190 Ah using a high pass filter

Figures 4.15 and 4.16 show that the parameter and $SOC$ estimates converge to the reference values accurately. This occurs because the low frequency errors are filtered out by the high-pass filter. One can also observe deviations in the $SOC$ estimate initially, especially for the case with a $\widehat{SOC}_0$ of 0.7. This occurs because the $\widehat{OCV}_{pre}^{err}$ signal shown in Figure 4.17 takes some time to converge to 0 in the time domain and is quite significant in magnitude as compared to the filtered $U_1$ signal initially, thus affecting the final $SOC$ estimate.

Also, it is seen that the estimate $\widehat{R}_0$ has an error at t = 40 min in both the figures. This is a consequence of the step introduced in parameter $A$ in the cell plant model. Since both $\widehat{A}$ and $\widehat{B}$ are feed-backed to estimate $R_0$, there are errors in $\widehat{R}_0$ when there are errors in $\widehat{A}$ and $\widehat{B}$, and after these estimates converge to the actual values of $A$ and $B$, the error disappears in $\widehat{R}_0$.

It is important to point out that sudden parameter variations in the cell can also be indicators of a thermal event. In this work, however, the primary focus of electrical errors at the cell level is the short circuit resistance $R_{ISCr}$, and this will be estimated in the following section.

## 4.5 Capacity $Q$ and $R_{ISCr}$ estimation

In the previous section, the results of the $SOC$ and parameter estimator were presented. In this section, the results of the capacity $Q$ and $R_{ISCr}$ estimates, using the $SOC$ estimate $\widehat{SOC}$ will be presented. First, the $\widehat{SOC}$ for four different values of $R_{ISCr}$ introduced into the plant model is depicted in Figure 4.18. The $\widehat{SOC}_0$ con-

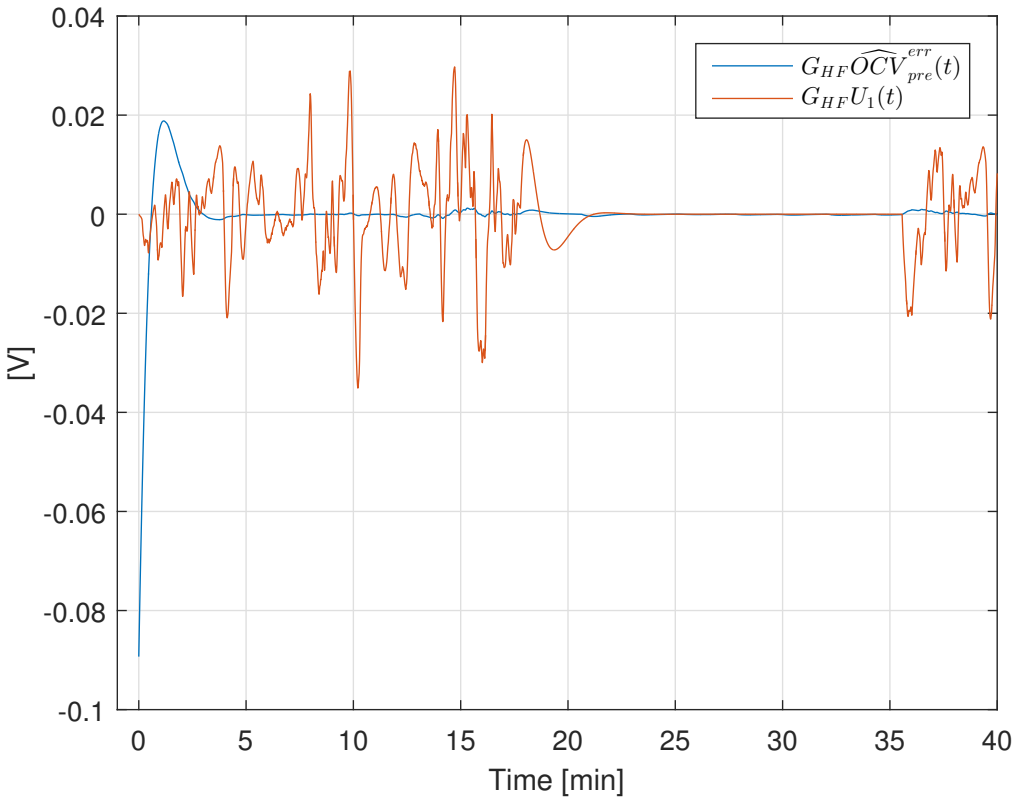


**Figure 4.17:** $G_{HF}U_1$ and $\widehat{OCV}^{err}_{pre}$ in the time domain for a $\widehat{SOC}_0$ of 0.7

sidered is 0.82, and the capacity $\widehat{Q_{nom}}$ in the estimator is 190 Ah, while the actual capacity of the cell is 180 Ah.

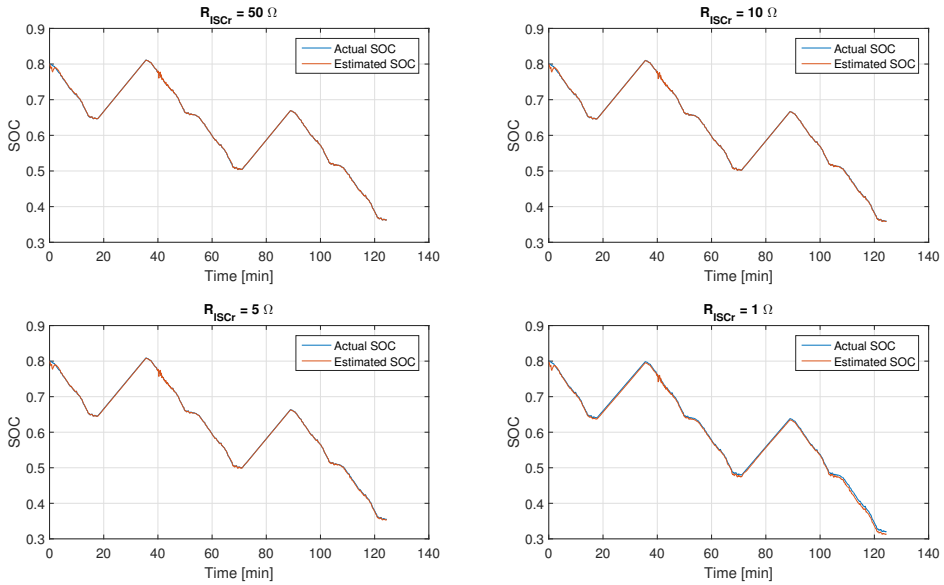


**Figure 4.18:** *SOC* estimate for various values of $R_{ISCr}$

The $SOC$ estimates of Figure 4.18 are quite close to the actual $SOC$ of the cell, and the estimation of $Q$ and $R_{ISCr}$ can now be formed using the method presented in section 3.6. Table 4.3 depicts the results of the estimation process for the four different $R_{ISCr}$ values using the Ordinary Least Squares method.

**Table 4.3:** Results of $Q$ and $R_{ISCr}$ estimation using the ordinary least squares algorithm $\hat{SOC}_0$ of 0.82

| Actual $R_{ISCr}$ | $\widehat{Q}$ | $\widehat{R}_{ISCr}$ |
|---|---|---|
| 50 Ω | 180.04 Ah | 35.71 Ω |
| 10 Ω | 179.96 Ah | 9.19 Ω |
| 5 Ω | 179.8 Ah | 4.79 Ω |
| 1 Ω | 178.34 Ah | 1.006 Ω |

The estimates $\widehat{Q}$ are very close to the actual value of 180 Ah, especially when the internal short is not very severe. As the short becomes more significant (for example 1 Ω), the capacity estimate worsens. It is also observed that $\widehat{R}_{ISCr}$ is close to the actual value, thus indicating that the extent of self-discharge can be monitored using such an estimation procedure.

The same estimation procedure is now repeated for a $\widehat{SOC}_0$ of 0.7. The results of the ordinary least squares estimator are presented in Table 4.4.

**Table 4.4:** Results of $Q$ and $R_{ISCr}$ estimation using the ordinary least squares algorithm for a $\widehat{SOC}_0$ of 0.7

| Actual $R_{ISCr}$ | $\widehat{Q}$ | $\widehat{R}_{ISCr}$ |
|---|---|---|
| 50 Ω | 179.93 Ah | 5.79 Ω |
| 10 Ω | 179.84 Ah | 3.96 Ω |
| 5 Ω | 179.69 Ah | 2.85 Ω |
| 1 Ω | 178.22 Ah | 0.89 Ω |

The values of $\widehat{R}_{ISCr}$ are quite off from the actual values. This happens because the OLS algorithm is very sensitive to outliers in data, which can be observed in the $\widehat{SOC}$ in Figure 4.16 near t = 0 min. The robust LS algorithm can be used to decrease the influence of outliers, and the estimation results using this algorithm are seen in Table 4.5. The estimation results can be observed to be significantly better as compared to Table 4.4.

**Table 4.5:** Results of $Q$ and $R_{ISCr}$ estimation using the robust least squares algorithm for a $\widehat{SOC}_0$ of 0.7

| Actual $R_{ISCr}$ | $\widehat{Q}$ | $\widehat{R}_{ISCr}$ |
|---|---|---|
| 50 Ω | 179.99 Ah | 30.16 Ω |
| 10 Ω | 179.89 Ah | 8.76 Ω |
| 5 Ω | 179.73 Ah | 4.64 Ω |
| 1 Ω | 178.24 Ah | 1 Ω |

# 5
# Discussion

In this chapter, the results will be scrutinized further to provide descriptions of potential uncertainties and deficiencies in this work and to also provide further commentary.

## 5.1 Comparative analysis based fault detection

The comparative analysis based fault detection schemes offer a simple and reliable solution to detect electrical faults occurring in a single cell in the pack. However, the OCV estimate that was obtained for the cells in the pack seems to be underestimated as compared to the actual OCV in the cell as was seen in Figure 4.3, which might be an issue if accurate OCV estimates are desired. This issue can be resolved by employing an RLS filter that uses a higher order battery model as described in detail in [32], although the estimation process can be more challenging with more parameters. Furthermore, it is assumed that the cells in a battery pack are largely similar in performance with no major differences in their parameters for the comparative analysis to function effectively and not be susceptible to false positives. In case a more individual cell level fault detection scheme is desired, techniques involving $R_{ISCr}$ estimation can be applied to each cell for the purpose of fault detection. The technique with OCV extraction using an RLS filter with a zeroth-order model has been successful in estimating $R_{ISCr}$ in [21] but was found to be unsatisfactory in this work, thereby warranting a more sophisticated approach.

The same method was also tested for faults in a single cell in a logical cell unit that was built in Simscape. The results were satisfactory for faults of a higher severity but were not conclusive for an $R_{ISCr}$ of 5 $\Omega$ and above as compared to the detection scheme applied to a single lumped cell. However, one can consider that even 1 $\Omega$ faults are minor in relationship to the internal resistance of a few $m\Omega$ in the cell and a load current that is of the order of 100 A.

In order to detect abnormal self-discharge over a long span of time, linear fits were performed on the terminal voltages on all the cells in the battery pack. The obvious disadvantage with this method is that the data over the chosen window period has to be stored for all cells, although one could argue that memory is not a grave consideration in recent years. A recursive linear regression can be implemented in case available memory is constrained.

A temperature based analysis can also be used for detection of internal short circuits as heat is generated as a consequence of such faults. However, temperature effects of an internal short can take a long time to appear on the surface of the cell thus making instantaneous detection difficult Furthermore, there is also continuous cooling both by the coolant and also external agents like wind when driving, thus affecting effective detection. Also, usually there are no temperature sensors for every cell thus rendering it difficult to establish a correlation between temperature increase and short in a specific cell. Further analysis needs to be performed to assess the merits of a thermal model based detection strategy.

## 5.2 High pass filter based parameter, $SOC$, capacity and $R_{ISCr}$ estimation

The previous methods performed fault detection without estimation of the $R_{ISCr}$. In this technique, the parameters and $SOC$ of the cell are estimated accurately using a high-pass filter to filter out low frequency errors. Although the primary focus is to obtain the $R_{ISCr}$ from the $SOC$ estimate, it is important to mention that other estimates such as capacity, ohmic resistance $R_0$ and polarization branch parameters $A$ and $B$ can also be used to identify abnormalities. For instance, an abrupt change in capacity or parameter estimates can be a potential indicator of the thermal run-away.

In the parameter and $SOC$ estimation block, the tuning parameters such as the initial covariance and the forgetting factor for all the RLS filters are chosen by trial and error. They have not been optimized in any way, for instance, to minimize the RMSE of the estimate for a particular chosen reference. Furthermore, $\Delta I$ and $\Delta T$ in the $R_0$ estimation block have been chosen purely based on visual observation and trial and error. The effect of sensor noise on the parameter estimates is not rigorously explored but the importance of having an excitation condition is specified in the context of the presence of sensor noise.

The capacity $Q$ and $R_{ISCr}$ estimation are performed in a non-recursive manner in this report. Recursive methods such as the Kalman filter and RLS to estimate these quantities were attempted, but it was observed that the estimates were highly sensitive to errors in the $SOC$ estimate. For example, when a parameter reference step was introduced in $A$, the estimate takes a while to attain steady state and during that time there is a disturbance in the $SOC$ estimate. This disturbance leads to issues in the recursive capacity estimator. It was attempted to solve this by tuning the process and measurement noise of the designed Kalman filter and forgetting factor of the RLS filter appropriately but it was not very successful. A possible fix would be to optimize the forgetting factors of the RLS filters for $R_0$, $A$ and $B$ estimation to push the $\widehat{SOC}$ disturbance to a higher frequency region, which can then be filtered out using a low pass filter. At present, the disturbance is not in a distinctly separate frequency band and thus, a Least Squares regression was used to estimate $SOC$ and $R_{ISCr}$.

## 5.3 Sustainable aspects

The implications of a thermal runaway on a cell form the economical perspective are easily understood. For instance, the thermal failures in the being aircraft [4] led to reputation damage and extensive investigation which proved very expensive. Lithium-ion batteries are gaining reputation in the electric vehicles area as a reliable source of energy, but safety incidents can prove very expensive for a company and in worst cases, might lead to call backs and halted sales. However, it is also important to ensure that any kind of a detection scheme does not lead to false positives as this can also lead to waste of resources and reputation if it happens often. In this work, several methods with different degrees of sophistication are presented and a combination of them can be used to minimize instances of false detection. Furthermore, it is important to contemplate the degree of sophistication of the detection scheme that is proposed, to ensure that the cheapest solution for effective detection is implemented.

The transition to a new technology is always met with skepticism. In order to overcome the initial social resistance to a new product, trust and reliability are very essential. In case safety critical incidents are reported with respect to batteries, even if they aren't very many, the social barrier for adoption of battery vehicles will grow and the ecological benefits of such vehicles will be ignored. Hence, it is imperative to invest in technology that makes electric vehicles and batteries trustworthy. A striking example of this is the Samsung phone explosion that occurred due to the battery [5] resulting in customer outrage and breach of trust, not to mention the widespread media coverage and damage to reputation. To summarize the social aspects, safety and preservation of human life must be top priority for any kind of technology and this work serves to achieve that in the context of electric vehicles.

There are no immediately obvious environmental impacts of implementing appropriate fault detection schemes for batteries besides the indirect benefits. However, as mentioned before, social acceptance and trust in electric vehicles ensures more sales and seamless transition, thereby ensuring ecological benefits of such technology with respect to emissions, noise etc.

## 5.4 Ethical aspects

In the context of IEEE's guidelines on ethical obligations that must be followed by engineers, three guidelines are chosen and elaborated further.

- To be honest and realistic in stating claims or estimates based on available data;

This project work is centred around making predictions and estimations based on available data and therefore, this guideline is especially relevant. It was important to verify that the parameters and look up tables used in the model are checked for correctness as they impact the algorithms significantly. Also, the input current profile was important to be chosen from a realistic scenario. Furthermore, in case any algorithm failed to identify faulty situations effectively, it was mentioned clearly in the chapter on results.

- To maintain and improve our technical competence and to undertake technological tasks for others only if qualified by training or experience, or after full disclosure of pertinent limitations;

  This work involved learning and familiarizing with many new techniques and therefore, improving competence was always a part of the process. At times, there was a risk of not maintaining a sufficient level of commitment towards that cause, but it was overcome for the most part. Integrity with respect to boundaries of knowledge and experience were kept to as significant an extent as possible, and assistance was sought when necessary especially with the algorithm involving a high-pass filter. The limitations of the various algorithms have been attempted to be captured as much as possible in the discussions chapter.

- To seek, accept, and offer honest criticism of technical work, to acknowledge and correct errors, and to credit properly the contributions of others

  Many of the tasks involved in this project were highly collaborative in nature, and involved extremely valuable inputs from others. There were instances where certain assumptions made initially were not perfectly valid, and subsequently had to be corrected as pointed out by supervisors. Feedback and criticism was also constantly sought and received with the ultimate goal of incorporation into the work.

# 6
# Conclusion

In this work, electrical faults in the battery cell unit are simulated and various algorithms for detection have been proposed. Specifically, the internal short circuit is considered for analysis and a plant model for the 1 RC link equivalent circuit of the battery cell with a modification to simulate a fault is employed. A Simscape plant model consisting of three individual cell units in parallel is also designed to simulate faults. The methods for fault detection detection using a comparative analysis without short circuit resistance ($R_{ISCr}$) estimation over the cells in the pack give satisfactory detection for internal shorts as soft as 5 Ω. Furthermore, the detection time is not very long thereby ensuring quick isolation of the fault. When the Simscape plant model is used with a fault on one of the parallel cell units, this detection is less satisfactory for the same severity of fault. A simple technique to detect abnormal self-discharge using a linear fit on the terminal voltage measurements is also evaluated, and it is observed clearly that the faulty cell can be detected through observation of the offset and slope.

Subsequently, a $SOC$ and parameter estimation procedure using frequency separation is designed and evaluated with the end goal of estimation of $R_{ISCr}$. Investigation of the frequency domain of the various signals is performed to determine filter properties and other aspects of design. The results of $SOC$ and parameter estimates for two different conditions of initial $SOC$ and capacity fed to the estimator depict clearly how low frequency errors propagate through the estimator and cause significant errors in these estimates. The high-pass filters eliminate these low frequency errors in the parameter estimators, thus giving much better estimates which are then used to calculate $SOC$ over the entire frequency range. The $SOC$ estimate after employing the filters are very accurate, with minor disturbances in the initial transient phase and also when parameter steps are introduced in the plant. The $R_{ISCr}$ and capacity $Q$ are estimated using a Least Squares and a modified Robust Least Squares technique for various scenarios. The estimation is observed to be reasonable, especially with the Robust Least Squares estimator that disregards outliers.

## 6.1 Future Work

There are several possible avenues to further improve or modify the detection algorithm design presented in this work.

- Since the comparative methods for fault detection involve $OCV$ extraction, other methods can be investigated to estimate the same. For instance, an RLS filter applied on a model with 1 RC link or a Kalman filter can be used.

- Voltage and current sensor noise can be introduced in the simulations to determine effects on the comparative analysis. Characterization of the sensors must first be done to obtain realistic values for the same.

- In the $SOC$ and parameter estimator, the forgetting factors and other design parameters can be obtained through optimization techniques.

- The effect of sensor noises has to be investigated on the performance of frequency separation estimator. This analysis is very important with respect to validating this method.

- The $R_{ISCr}$ and capacity $Q$ estimator is not implemented recursively in this work. This must be investigated further, with respect to isolation of frequency bands where the disturbances in the $SOC$ estimate are not present. This also relates to optimization of the forgetting factor for the parameter estimators to give a faster rise time, so the $SOC$ estimate has smaller disturbances.

- A thermal analysis can be performed using thermal models of the cells on FEM software or Simulink to determine feasibility of soft short circuit detection using temperature measurements. The specific architecture of temperature sensors in the pack and other must be incorporated into the analysis.

# Bibliography


[1] D. Pelegov and J. Pontes, "Main Drivers of Battery Industry Changes: Electric Vehicles—A Market Overview", *Batteries*, 2018, ISSN: 2313-0105. DOI: 10.3390/batteries4040065.

[2] R. Sprague, "An Analysis of Current Battery Technology and Electric Vehicles", Tech. Rep., 2015, p. 1.

[3] "EAG.COM MATERIALS SCIENCES", Tech. Rep., 2017. [Online]. Available: http://www.plugincars.com/cars..

[4] J. M. Kolly, J. Panagiotou, and B. A. Czech, "The Investigation of a Lithium-Ion Battery Fire Onboard a Boeing 787 by the US National Transportation Safety Board", Tech. Rep.

[5] "Galaxy Note 7 Battery Autopsy and Analysis Background and the Public Picture", Tech. Rep.

[6] X. Feng, M. Ouyang, X. Liu, L. Lu, Y. Xia, and X. He, *Thermal runaway mechanism of lithium ion battery for electric vehicles: A review*, 2018. DOI: 10.1016/j.ensm.2017.05.013.

[7] X. Liu, D. Ren, H. Hsu, X. Feng, G. L. Xu, M. Zhuang, H. Gao, L. Lu, X. Han, Z. Chu, J. Li, X. He, K. Amine, and M. Ouyang, "Thermal Runaway of Lithium-Ion Batteries without Internal Short Circuit", *Joule*, 2018, ISSN: 25424351. DOI: 10.1016/j.joule.2018.06.015.

[8] Y. Wu, S. Saxena, Y. Xing, Y. Wang, C. Li, W. K. Yung, and M. Pecht, "Analysis of manufacturing-induced defects and structural deformations in lithium-ion batteries using computed tomography", *Energies*, 2018, ISSN: 19961073. DOI: 10.3390/en11040925.

[9] D. P. Finegan, M. Scheel, J. B. Robinson, B. Tjaden, M. Di Michiel, G. Hinds, D. J. Brett, and P. R. Shearing, "Investigating lithium-ion battery materials during overcharge-induced thermal runaway: An operando and multi-scale X-ray CT study", *Physical Chemistry Chemical Physics*, 2016, ISSN: 14639076. DOI: 10.1039/c6cp04251a.

[10] R. Guo, L. Lu, M. Ouyang, and X. Feng, "Mechanism of the entire overdischarge process and overdischarge-induced internal short circuit in lithium-ion batteries", *Scientific Reports*, 2016, ISSN: 20452322. DOI: 10.1038/srep30248.

[11] G. H. Kim, K. Smith, J. Ireland, and A. Pesaran, "Fail-safe design for large capacity lithium-ion battery systems", *Journal of Power Sources*, 2012, ISSN: 03787753. DOI: 10.1016/j.jpowsour.2012.03.015.

[12] S. Koch, K. Birke, and R. Kuhn, "Fast Thermal Runaway Detection for Lithium-Ion Cells in Large Scale Traction Batteries", *Batteries*, 2018, ISSN: 2313-0105. DOI: 10.3390/batteries4020016.

[13] S. V. Sazhin, E. J. Dufek, and K. L. Gering, "Enhancing Li-Ion Battery Safety by Early Detection of Nascent Internal Shorts", *Journal of The Electrochemical Society*, 2017, ISSN: 0013-4651. DOI: 10.1149/2.0431701jes.

[14] Z. Liu and H. He, "Model-based sensor fault diagnosis of a lithium-ion battery in electric vehicles", *Energies*, 2015, ISSN: 19961073. DOI: 10.3390/en8076509.

[15] M. Ouyang, M. Zhang, X. Feng, L. Lu, J. Li, X. He, and Y. Zheng, "Internal short circuit detection for battery pack using equivalent parameter and consistency method", *Journal of Power Sources*, pp. 272–283, 2015. DOI: 10.1016/j.jpowsour.2015.06.087.

[16] X. Feng, C. Weng, M. Ouyang, and J. Sun, "Online internal short circuit detection for a large format lithium ion battery", *Applied Energy*, 2016, ISSN: 03062619. DOI: 10.1016/j.apenergy.2015.10.019.

[17] A. Singh, A. Izadian, and S. Anwar, "Model based condition monitoring in lithium-ion batteries", 2014. DOI: 10.1016/j.jpowsour.2014.06.052. [Online]. Available: http://dx.doi.org/10.1016/j.jpowsour.2014.06.052.

[18] A. Sidhu, A. Izadian, and S. Anwar, "Model-Based Adaptive Fault Diagnosis in Lithium Ion Batteries: A Comparison of Linear and Nonlinear Approaches", Mar. 2017. DOI: 10.4271/2017-01-1192. [Online]. Available: http://papers.sae.org/2017-01-1192/.

[19] M. A. Rahman, S. Anwar, and A. Izadian, "Electrochemical Model Based Fault Diagnosis of Lithium Ion Battery", *Advances in Automobile Engineering*, 2016, ISSN: 21677670. DOI: 10.4172/2167-7670.1000159.

[20] M. Seo, T. Goh, G. Koo, M. Park, and S. W. Kim, "Detection of Internal Short Circuit in Li-ion Battery by Estimating its Resistance", in *Proceedings of the 4th IIAE International Conference on Intelligent Systems and Image Processing 2016*, 2016, ISBN: 9784907220105. DOI: 10.12792/icisip2016.038.

[21] M. Seo, T. Goh, M. Park, G. Koo, and S. W. Kim, "Detection of internal short circuit in lithium ion battery using model-based switching model method", *Energies*, 2017, ISSN: 19961073. DOI: 10.3390/en10010076.

[22] M. Seo, T. Goh, M. Park, and S. Woo Kim, "Detection Method for Soft Internal Short Circuit in Lithium-Ion Battery Pack by Extracting Open Circuit Voltage of Faulted Cell", *Energies*, 2018. DOI: 10.3390/en11071669.

[23] C. Zhang, K. Li, S. McLoone, and Z. Yang, "Battery modelling methods for electric vehicles - A review", in *2014 European Control Conference, ECC 2014*, 2014, ISBN: 9783952426913. DOI: 10.1109/ECC.2014.6862541.

[24] Z. Deng, L. Yang, Y. Cai, and H. Deng, "Maximum Available Capacity and Energy Estimation Based on Support Vector Machine Regression for Lithium-ion Battery", in *Energy Procedia*, 2017. DOI: 10.1016/j.egypro.2016.12.131.

[25] Q. Zhong, B. Huang, J. Ma, and H. Li, "Experimental study on relationship between SOC and OCV of lithium-ion batteries", Tech. Rep.

[26] A. Farmann and D. U. Sauer, "A study on the dependency of the open-circuit voltage on temperature and actual aging state of lithium-ion batteries", *Journal of Power Sources*, 2017, ISSN: 03787753. DOI: 10.1016/j.jpowsour.2017.01.098.

[27] M. A. Roscher, O. Bohlen, and J. Vetter, "OCV Hysteresis in Li-Ion Batteries including Two-Phase Transition Materials", *International Journal of Electrochemistry*, 2011, ISSN: 2090-3537. DOI: 10.4061/2011/984320.

[28] M. Schwartz, "Deposition from Aqueous Solutions: An Overview", Tech. Rep.

[29] L. Zhang, H. Peng, Z. Ning, Z. Mu, and C. Sun, "Comparative Research on RC Equivalent Circuit Models for Lithium-Ion Batteries of Electric Vehicles", *Applied Sciences*, 2017, ISSN: 2076-3417. DOI: 10.3390/app7101002.

[30] C. Bierich, C. Nagaraj, E. Magnusson, F. Idegård, N. Höglund, and V. Basker, "Characterization and Modeling of a Lithium-Ion Supercapacitor, An Analytic Investigation of a Novel Energy Storage Device", Tech. Rep.

[31] T. G. Zavalis, M. Behm, and G. Lindbergh, "Investigation of Short-Circuit Scenarios in a Lithium-Ion Battery Cell", *Journal of The Electrochemical Society*, 2012, ISSN: 00134651. DOI: 10.1149/2.096206jes.

[32] H. He, X. Zhang, R. Xiong, Y. Xu, and H. Guo, "Online model-based estimation of state-of-charge and open-circuit voltage of lithium-ion batteries in electric vehicles", *Energy*, 2012, ISSN: 03605442. DOI: 10.1016/j.energy.2012.01.009.

[33] B. Lindoo, "On the Optimal Choice of the Forgetting Factor in the Recursive Least Squares Estimator", Tech. Rep., 1997.